Stimulus statistics and HCN current mediated resonance sets the scale of input-output mapping in Stellate cells of the Medial Entorhinal Cortex

Nupur Katyare & Sujit Sikdar
Molecular Biophysics Unit, Indian Institute of Science, Bangalore, India, 560012.

Abstract

The functional significance of the computations performed by Stellate cells of the Medial Entorhinal Cortex, proven time and again, makes them insightful, yet intriguing. The gradients of the intrinsic properties of these cells, aligned to the actual grid cell spacing gradients, have encouraged many thoughtful experiments. A long sought question in the stellate cell literature is thus the one seeking mechanistic implications for these correlates. The intrinsic dynamics of these cells have been tested previously in this light, primarily focusing on their spectral characteristics. However, the resonance phenomenon underlying these dynamics has not received the attention it deserves, and its potency under the in-vivo high conductance states to influence the input-output mapping remains to be estimated. In this light, we analyzed the signal gain of stellate cells in the presence of in-vivo like fluctuating conductance based synaptic inputs injected through the Dynamic clamp, in rat brain slices. We observed a consistent, HCN current sensitive, theta frequency peak in signal gain, indicating that the HCN current mediated resonance mechanisms are functional even under a heavy input barrage. Next, we tested the effects of an array of input statistics on this signal gain and observed it to be mostly unaffected by the input strength, but relatively susceptible to the input kinetics. Additionally, as a possible reflection of the underlying signal gain, we observed a significant theta modulation of inputs by HCN current, the extent of which was found to be influenced by the excitatory, but not inhibitory synaptic kinetics. Surprisingly, a corresponding modulation in the gamma frequencies was also observed for the firing rate response, wherein the signal gain in gamma frequencies was found to be higher in the presence of HCN, which also coincided with increased occurrence of bursts.
A computational model with HCN-persistent sodium channels with similar simulated in vivo conditions could reproduce the experimental results, additionally suggesting the strength of inhibition and the kinetics of excitation as the input statistic based alternate resonance mechanisms which can operate independent of HCN.
Our results thus suggest frequency dependent gain as an appropriate measure for analyzing the input-output mapping in the stellate cells, and point out the mechanisms via which the HCN currents and input statistics can interact and determine the scaling of responses in these cells.

Introduction

The computational capabilities of Stellate cells of the Medial Entorhinal Cortex (MEC) are evident from their grid-like and border-like spatial representations (Domnisoru, Kinkhabwala, and Tank 2013; Christoph Schmidt-Hieber and Häusser 2013; Tang et al. 2014), their necessity for spatial learning (Tennant et al. 2018), their

ability to facilitate contextual representations in the downstream circuits (Sun et al. 2015), steeper slopes of phase precession (Reifenstein et al. 2016), and their possible contributions to the theta and the gamma rhythms (Quilichini, Sirota, and Buzsáki 2010).

Although other excitatory cell types have now been reported to exhibit grid-like firing patterns (Boccara et al. 2010; Tang et al. 2014), the strong correlation between the gradient of intrinsic properties and integration time window of stellate cells along the dorsoventral axis of the Medial Entorhinal Cortex (MEC), and a similar gradient observed in the spacing of the grid fields (Brun et al. 2008; Garden et al. 2008; Giocomo et al. 2007; Giocomo and Hasselmo 2008; Moser, Kropff, and Moser 2008; Navratilova et al. 2012), is still in need of many mechanistic and theoretical explanations.

Theories explaining spatial periodicity generally link these gradients by assuming a mapping between the speed-direction modulated inputs, and the consequent modulation of the membrane voltage response; accounting for the path integration (Garden et al. 2008; Jeewajee et al. 2008; McNaughton et al. 2006; Narayanan and Johnston 2008; Navratilova et al. 2012; C. Schmidt-Hieber and Hausser 2013).

Such a mapping, in general, can emerge through certain peculiarities in the intrinsic properties of neurons in this region (Hasselmo and Brandon 2008; Jeewajee et al. 2008; Remme, Lengyel, and Gutkin 2010), a distinct network architecture (Couey et al. 2013; McNaughton et al. 2006) or a characteristic flux of inputs to this network (Justus et al. 2016; Kropff et al. 2015).

The intrinsic mechanisms in stellate cells thought to affect the mapping between speed modulated excitation and the firing response are mainly the intrinsic theta oscillations (Barry et al. 2012; Burgess, Barry, and Keefe 2007; Jeewajee et al. 2008), other HCN channels mediated mechanisms (Ferrante et al. n.d.; Garden et al. 2008) and the membrane resistance and its effects on the time constants (Garden et al. 2008; Navratilova et al. 2012).

These are owing to the facts that aligned to the D-V gradient of grid spacing (Brun et al. 2008), gradients of frequency of intrinsic oscillations (Giocomo et al. 2007), HCN current (Garden et al. 2008), HCN time constant (Giocomo and Hasselmo 2008), and membrane resistance (Garden et al. 2008) are also present. Intrinsic theta oscillations, although their presence under in-vivo conditions was previously questioned (Fernandez and White 2008), have been confirmed in in-vivo intracellular recordings of the grid cells (Domnisoru, Kinkhabwala, and Tank 2013). These under in-vitro recordings of stellate cells have been shown to be sensitive to the HCN current (Dickson et al. 2000). The involvement of HCN channels is also evident from the experiments on the HCN1 KO mice, where the grid scale was found to be expanded, and the slope of the theta frequency modulation by speed was reduced (Giocomo et al. 2011). Theories of grid pattern formation which thus incorporate HCN channels, generally consider the role of HCN channels in either directly pacing the subthreshold oscillations (Giocomo et al. 2007) or in influencing the membrane resistance (R_m) and thus, the membrane time constant (τ_m) (Garden et al. 2008; Navratilova et al. 2012). However, the role of HCN channels in pacing subthreshold oscillations in-vivo, and the effects of HCN channels on membrane resistance under the in-vivo high conductance states are questionable (Mishra and Narayanan 2014; Nolan et al. 2007). This calls for a consideration of other mechanisms via which the HCN channels can possibly influence the input-output mapping under in-vivo states.

The ability of neurons to selectively amplify certain signals from the noisy inputs can greatly influence this mapping at multiple levels (Higgs and Spain 2009) and there is scope for considering that the HCN channel mediated frequency selectivity of stellate cells can efficiently contribute to such gain modulation. Such frequency response properties of stellate cells under in-vivo conditions have not yet been systematically characterized. In fact, even in other neurons where such estimates are made, current based inputs were used, and these studies were mostly carried out in the non-resonant systems (Higgs and Spain 2009).

The previous studies on in-vivo states have reported a significant gain reduction under these high conductance states (Chance, Abbott, and Reyes 2002) (which makes the theories based solely on the R_m-τ_m questionable); but these studies too, have not analyzed frequency dependent differential gain modulation.

To address these issues, we tested the frequency dependent gain in stellate cells of the MEC, subjected to in-vivo like high conductance bombardment generated through the dynamic clamp (A. Destexhe et al. 2001). We observed that HCN channels play a major role in confining the signal gain to theta-frequency even in the presence of a strong noise. We analyzed this signal gain for both the subthreshold responses and the rate modulation, and via systematically perturbing the stimulus statistics. And while studying the influence of inputs on the underlying resonance mechanisms, we observed that the inputs themselves are significantly modulated in theta frequency by HCN current.

We could confirm these results in a computational model of stellate cell subjected to the same input regime, which provided additional insights regarding the role of inhibitory strength and excitatory kinetics as alternate resonance mechanisms in the absence of HCN channels, which can underlie the spatial periodicity in other cell types. Our results thus point out the mechanisms via which the HCN channels and input statistics can interact to determine the neuronal signal gain and its dynamic adaptation, which can make the neuronal responses sensitive to subtle signals latent in input statistics, thus enriching the scale of neuronal representations.

Results:

Mimicking in-vivo states through the dynamic clamp

For assessing whether and how the mechanisms of resonance operate under the in-vivo high conductance states, we generated in-vivo like stochastic synaptic activity in stellate cells via the dynamic clamp (A. Destexhe et al. 2001). After assessing the basic electrophysiological characteristics in current clamp for the confirmation of stellate cell identity (Supplementary fig. S1) the recording mode was switched to the dynamic clamp. All the recordings were performed under the blockers for the native excitatory and inhibitory currents (see methods).

We could observe ~ 10 mV of membrane depolarization, large voltage fluctuations and a drastic drop in membrane resistance which are the hallmarks of the in-vivo states (A. Destexhe et al. 2001). To rule out the differential effects of excitatory and inhibitory synaptic time constants, and to account for the possibility of partially active slow NMDA currents, we used matched excitatory and inhibitory time constants (10 ms) for the initial recordings (Fig.1A), and studied the effects of variations in these kinetics separately in the latter experiments.

The mean as well as SD of inhibition used was twice that of the excitation (Fig.1B), which induced the observed depolarization and spontaneous firing. Stellate cells at this level of activity spontaneously started firing in theta frequency (Fig.1C). The underlying large voltage fluctuations were evident in the membrane potential histogram with SD of ~ 5 mV (Fig.1D).

Next, as reported previously (A. Destexhe et al. 2001), we observed that the input resistance dropped drastically (~ 70 %) under the in-vivo regime, and almost thrice the amount of original current was now required to achieve the similar depolarization (Fig.1E).

The synaptic parameters used for the in-vivo regime were now held fixed (see 'Default Parameters', methods), and unless otherwise clarified, were not tampered in the following experiments.

Theta frequency peak in signal gain

Next, we estimated signal gain of stellate cells when the cells were firing in theta frequency under the mimicked in-vivo states.

Two types of responses were considered, leading to two different signal gain waveforms. $Gain_V$, computed from the collective voltage trace (fig.2 Aa), and $Gain_R$ computed from the instantaneous firing rate vector (fig.3 A).

We observed a prominent peak in theta frequency in $Gain_V$ waveform (fig.2 B ctrl), which shifted significantly to lower frequencies after blocking HCN channels with ZD7288 (25 μM) (fig.2 B, ZD); although the firing rates in the control and test cases were comparable (fig.2, Ab).

This drift from theta frequency is indicative of the persistent potency of HCN current to impart resonance properties to neurons even under a heavy barrage of synaptic noise.

Next, to quantify the changes in gain waveform with ZD, we compared the frequency at which the peak was observed (f_{peak}), the actual gain at peak (G_{max}), and the relative gain in theta frequency (4-

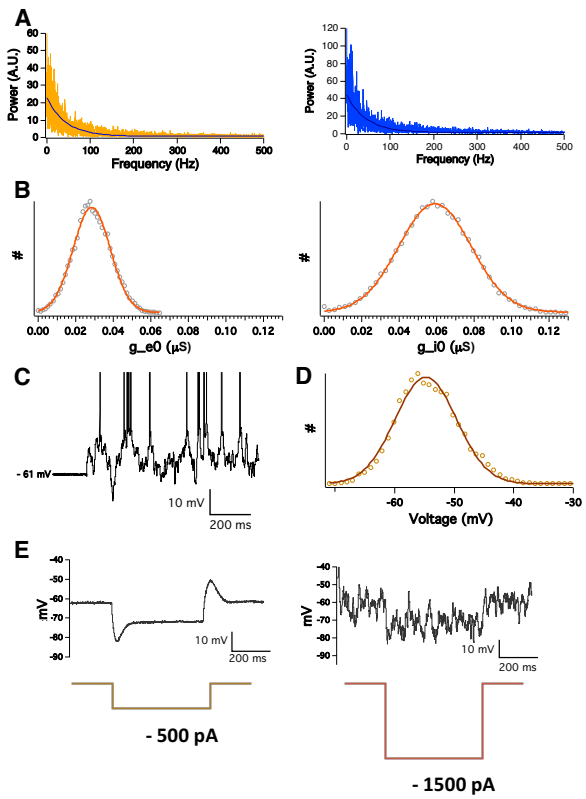

Fig. 1 Dynamic clamp mimicked In-vivo states
A. Power spectrum of the stochastic excitatory conductance (left), inhibitory conductance (right). B. Histogram of the stochastic excitatory conductance (left), inhibitory conductance (right). C. Large voltage fluctuations and spontaneous firing observed during in-vivo states. (Step-like depolarization owing to fast rise kinetics of the mean excitatory conductance). D. Membrane voltage histogram from the voltage trace in C, SD ~ 5 mV. E. Left: ~ 10 mV Steady state Voltage deflection from -500 pA current step before switching to the in-vivo regime, Right: Similar ~ 10 mV Steady state Voltage deflection from -1500 pA current step in the in-vivo regime.

14 Hz) (theta-index); across the control and the test cases. For the 12 cells tested, the f_{peak} showed a significant shift to lower frequencies, in the absence of HCN channels (Fig.2 C).

The actual gain (G_{max}) was slightly higher in test than the control conditions (Fig.2 D), which can be expected considering the effects of higher input resistance after blocking HCN channels. Interestingly, however, the relative theta-frequency gain (theta-index), computed as a ratio of the average gain in 4-14 Hz and the average gain in rest of the 0.5-1000 Hz, was significantly higher in control conditions that the test (Fig.2 E).

It should be noted here that although we have used a voltage trace inclusive of spikes for these analyses, which allowed us to check the actual perithreshold dynamics, the spikes were not contributing to the theta frequency gain directly and were mostly contributing slightly to the higher frequency gain (fig. S2) The slower modulations in firing pattern and the subthreshold responses, however, were more important in determining the gain over lower frequencies.

Next, to determine whether the observed subthreshold frequency selectivity can actually modulate the firing pattern of these cells, we computed $Gain_R$ from a firing rate vector constructed from a smoothly varying instantaneous firing rate (fig.3, A).

Interestingly, the $Gain_R$ waveform too displayed a prominent peak in theta frequency (fig.3, B ctrl), which shifted significantly to lower frequencies after blocking HCN channels (fig.3, B ZD).

Again, for the 12 cells tested, the shift of the gain peak in test conditions was significant (fig.3, C), but unlike for $Gain_V$, in case of $Gain_R$, the increase in G_{max} was non-significant (fig.3, D). Interestingly, the theta-index was still significantly higher for control than the test conditions (fig.3, E).

Also it should be noted, that, unlike previous reports using current based noise (Brunel et al. 2001; Higgs and Spain 2009), we did not observe any correlation between the $Gain_R$ f_{peak} and the mean firing rate (fig.3, F Left). Instead a weak correlation was observed between the $Gain_R$ f_{peak} and the cell's resonance frequency (fig.3, F middle).

The actual $Gain_R$ G_{max}, however, was observed to increase linearly with the firing rate (fig.3, F Right), indicating that the signal gain amplitude is sensitive to the actual response strength, but the spectral preferences are mediated by the underlying resonance mechanisms.

These findings are in accordance with the previous studies reflecting on the influence of the subthreshold resonance mechanisms on the active properties (Richardson, Brunel, and Hakim 2003), and suggest the frequency dependent gain as a suitable index for mapping the relationship between the sensory modalities mediated excitation and the resulting firing rate response; which has not received the deserved attention so far.

The estimation of signal gain thus provided us a way to observe the ongoing stimulus-response interactions. To assess the same in detail,

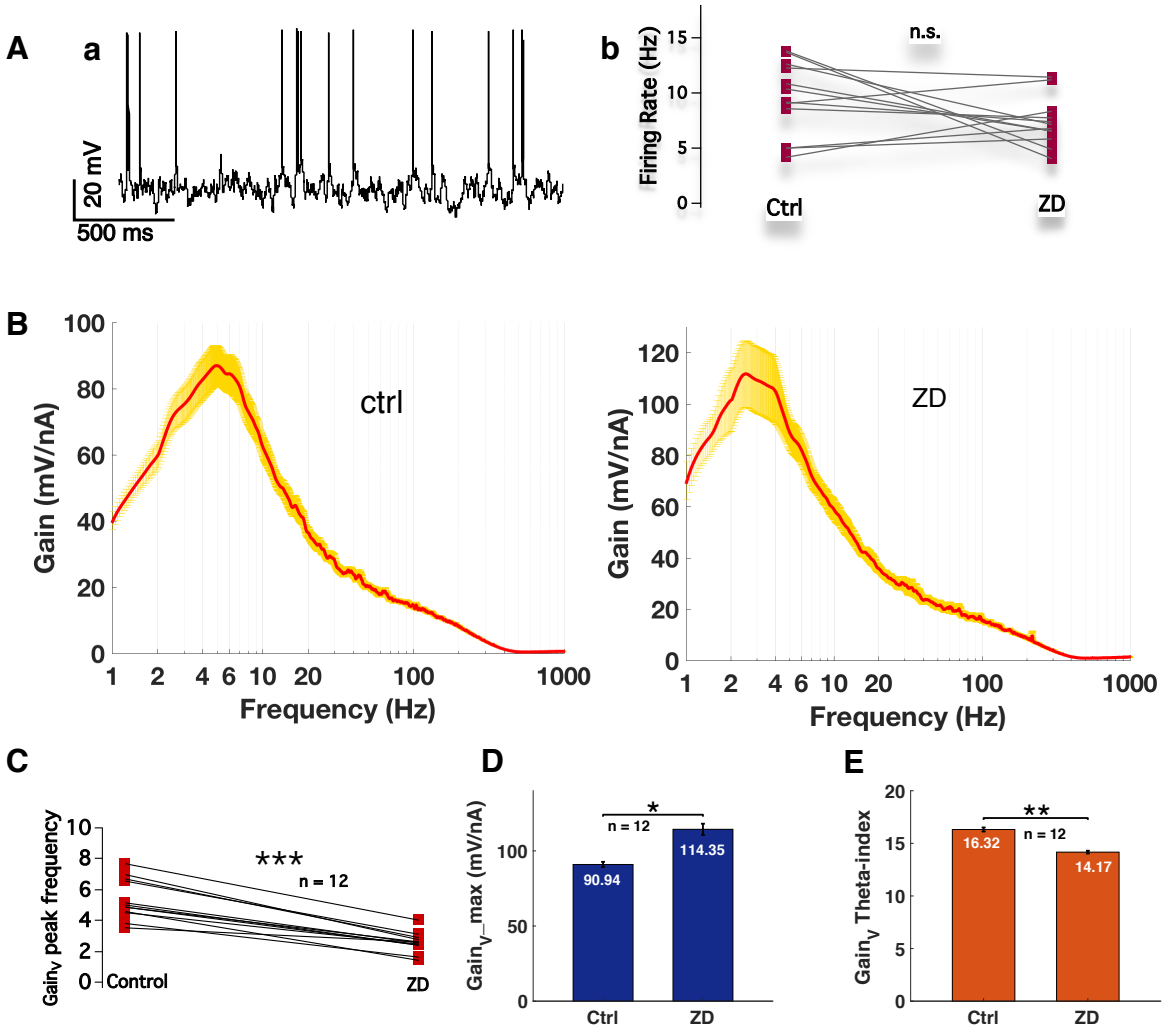

Fig. 2 Signal gain of stellate cells estimated from the collective voltage trace
A. a.Voltage response of a stellate cell during mimicked in-vivo states . Note spontaneous theta frequency firing and a detectable rhythmicity in voltage fluctuations. b.Comparison of the mean firing rates in the control and the test case B. Signal gain in the control case. (Left) and after blocking HCN channels with ZD7288 (Right). The plots represent average for 12 cells, error bars are SEM. C. Changes in the gain peak frequency for 12 cells in presence of ZD7288. D,E. Summary of the changes in the actual gain at peak (D) and theta-index (E) in the presence of ZD7288.
A,C,D,E: *** $p < 0.001$, ** $p < 0.01$, * $p < 0.05$, n.s., Student's paired t-test.

considering the previously suggested influence of input statistics on the neuronal signal gain (Brunel et al. 2001; Higgs and Spain 2009), we systematically changed the synaptic parameters of the in-vivo regime and re-estimated the frequency dependent gain.

Effect of the strength of excitation on the signal gain

To start with, for quantifying the changes in signal gain with the increased excitatory drive, we alternately varied the mean and SD of excitation few units around the default values used.

The mean firing rates increased linearly with the increase in mean or SD of excitation, which was intuitive. For the cells in which the HCN channels were blocked with ZD, the initial mean firing rates in control and test cases were comparable (~ 5Hz), and no significant differences in the slopes were observed for the increase thereafter (fig. 9A).

No significant changes with mean or SD of excitation were observed in the f_{peak}, or theta-index of $Gain_V$ or $Gain_R$ in control (fig.4 A,B) or with ZD (fig. S3).

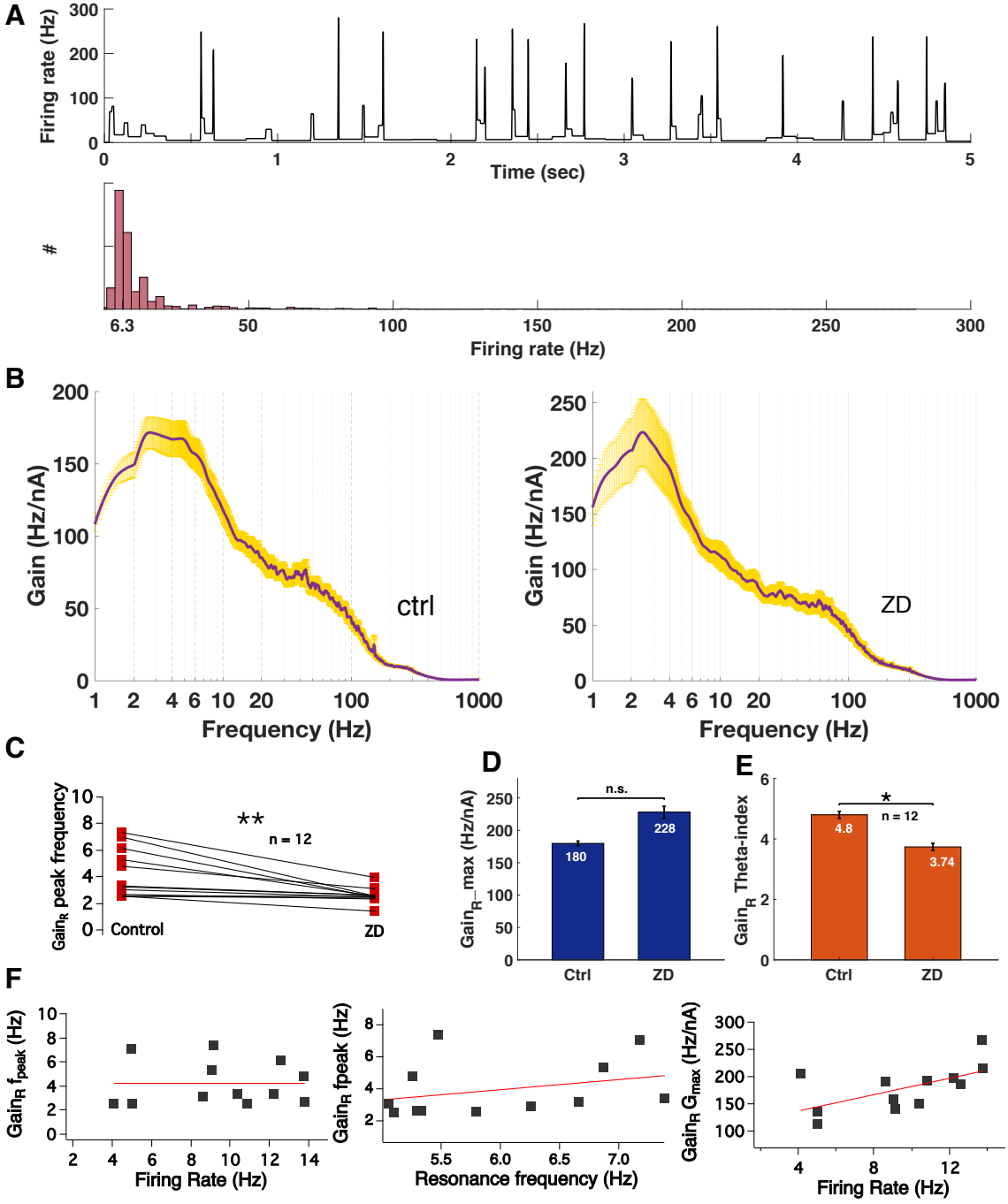

Fig. 3 Signal gain of stellate cells estimated from the firing rate response

A. Instantaneous firing rate as a function of time for the first 5 sec of a trial (Top), Histogram of the rate vector (Bottom). B. Signal gain in the control case (Left) and after blocking HCN channels with ZD7288 (Right). The plots represent average for 12 cells, error bars are SEM. C. Changes in the gain peak frequency for 12 cells in the presence of ZD7288. D,E. Summary of the changes in the actual gain at peak (D) and theta-index (E) in the presence of ZD7288. F. Correlaton between $Gain_R$ f_{peak} and firing rate (Left), $Gain_R$ f_{peak} and resonance frequency (Middle), $Gain_R$ f_{max} and firing rate (Right).

C,D,E: ** $p < 0.01$, * $p < 0.05$, Student's paired t-test; n.s. non-significant

The G_{max}, however, showed an interesting relationship with the excitatory strength. The $gain_V$ G_{max} decreased significantly with increase in SD of excitation in the control case for upto 75 % of the maximum SD used; but such a trend was not observed with ZD (fig.4 C). Also, $Gain_R$ G_{max} in control and the test case, although non-significant, followed a similar trend (fig.4 D).

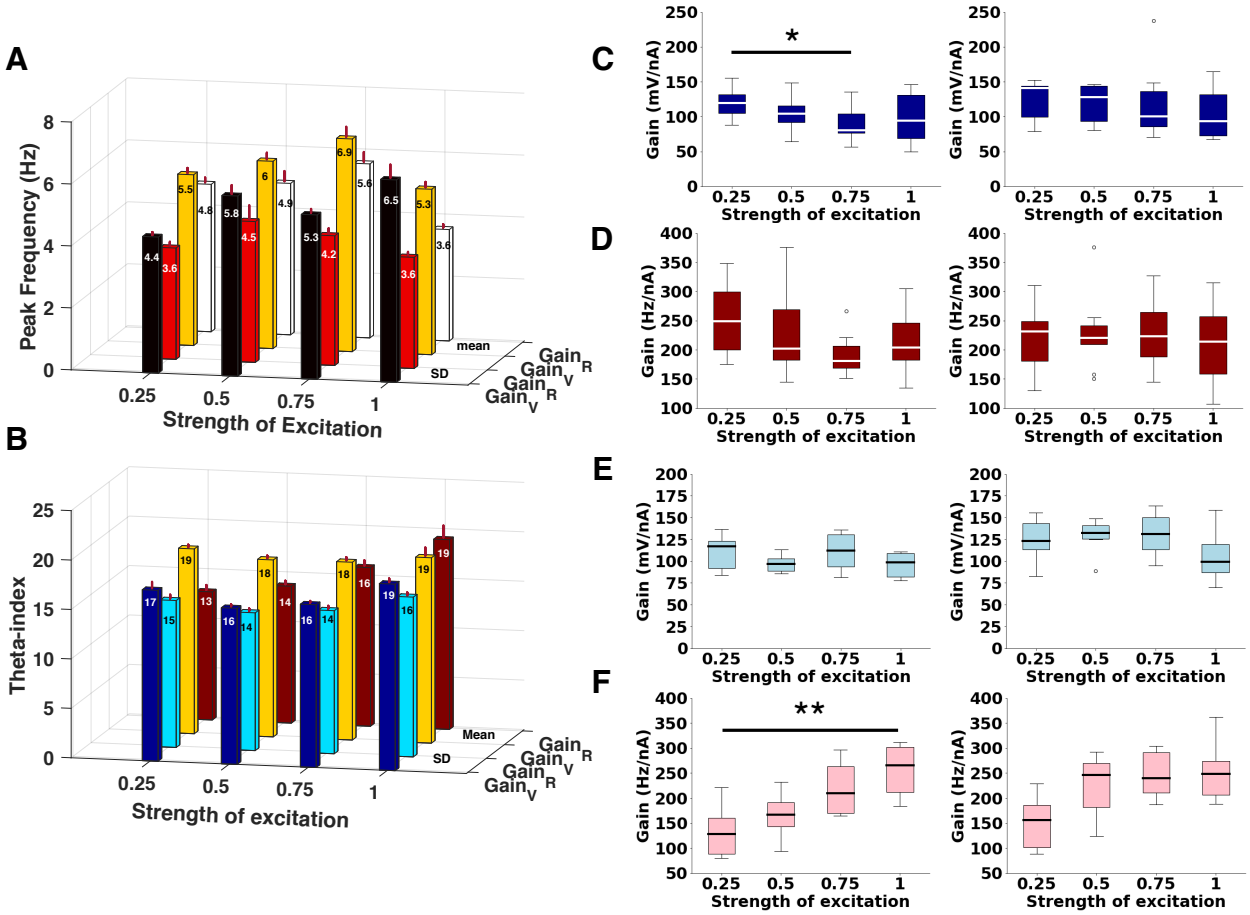

Fig. 4 Effects of strength of excitation on the signal gain

A. Variations in the peak frequency of gain$_V$ and gain$_R$ as a function of strength of excitation (normalized), after varying the mean or SD of excitatory conductance. B. Same as A for the theta-index C, D. Changes in the gain at peak for gain$_V$ (Top) and gain$_R$ (Bottom) as a function of SD of the excitatory conductance (normalized). E,F. Same as C,D for the mean of the excitatory conductance

C,F: ** $p < 0.01$, * $p < 0.05$, Kruscal-Wallis test; All others: non-significant, Kruscal-Wallis test.

With increase in the mean however, no significant changes in Gain$_V$ G_{max} could be observed (fig.4 E); but Gain$_R$ G_{max} increased significantly (fig.4 F Left). Again, this increase was not significant in the experiments with ZD (fig.4 F Right).

These results clearly indicate that HCN channels selectively increase the gain of subthreshold excitatory fluctuations, which thus decreases as the HCN channels deactivate with depolarization. The same is also evident from absence of such trend with ZD, where the HCN channels are already deactivated. These effects are not observed with the mean excitation, as although the contribution of HCN channels to the gain decreases with depolarization, the direct increase in the mean excitation balances out these effects. The significant increase in the Gain$_R$ G_{max} with the mean in control conditions can be explained by the fact that the overall theta-frequency gain, theta-index, in control conditions is already higher than the test (Fig.2 E, fig.3 E).

Effects of synaptic kinetics

Next, we repeated the gain measurements while making the kinetics of the synaptic stochastic process (excitatory as well as inhibitory) slower and slower, by changing the time constants of the conductances in steps of ~ 5, 10, 50 and 100 ms. In case of the fastest inputs, the excitation was adjusted to be slightly faster than inhibition (exc. 3, inh. 5); but for the next steps the time constants were held equal considering that the small difference used initially would be diluted.

The effects of slower input kinetics could be easily detected in the power spectrum of the voltage response itself, with its peak frequency shifting significantly to lower values with slower inputs (fig.6 D).

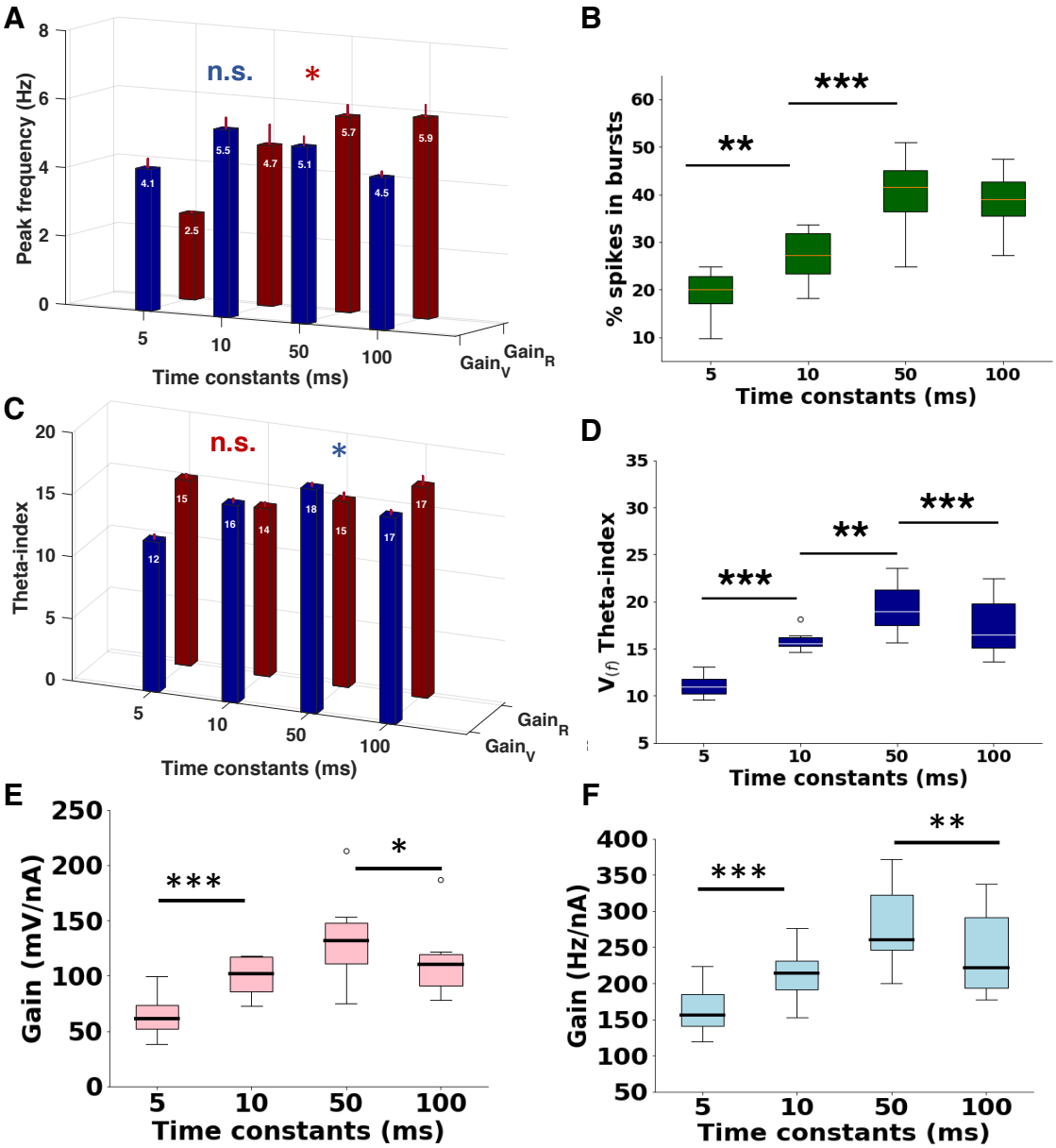

Fig. 5 Effects of input kinetics on the signal gain

A. Variations in the peak frequency of gain$_V$ and gain$_R$ as a function of input kinetics. B. Percentage of spikes occurring in bursts as function of input kinetics. C. Same as A for the theta-index D. Changes in the theta-index of power spectrum of the voltage response (average power in 4-14 Hz / average power in rest of the 0.5 -1000 Hz) with input kinetics. E,F. Variations in the gain$_V$ at peak (E) and gain$_R$ at peak (F) with input kinetics.

A,C: * $p < 0.05$, n.s. non significant, Kruscal-Wallis test; B,D-F: *** $p < 0.001$, ** $p < 0.01$, * $p < 0.05$, others: non significant, Student's paired t-test.

Interestingly, no such trend was observed in the gain$_V$ f_{peak}, and it was apparently unaffected by the input kinetics (fig.5 A).

The theta-index of the voltage power spectrum, however, was observed to increase significantly as the input kinetics changed from ~5 to 50 ms and then to decrease significantly from 50 to 100 ms (fig.5 D); possibly owing to an increased summation of excitatory inputs in the theta frequency upto 50 ms, and in slower frequencies thereafter.

Also, as a consequence possibly, the theta-index, and G_{max} of Gain$_V$ followed a similar trend with increase in input kinetics (fig.5 C, E).

Next, analyzing the suprathreshold responses, we observed that the mean firing rate, while still

being in theta frequency, decreased significantly as the time constants increased beyond 10 ms (fig. S4 A), indicating significantly slower rate modulation. Surprisingly however, in spite of this decrease in the mean firing rate, the f_{peak} of $Gain_R$, showed an interesting overall increase (fig.5 A). One of the underlying factors causing this can be the higher frequency bursts, which, apart from increasing the gamma frequency power, when modulated in theta frequency, can give rise to an overall increase in power in theta frequency. To test this, we analyzed the percentage of spikes occurring as bursts (frequency > 50 Hz) for each group, and indeed observed that the bursts increased significantly as the synaptic time constants increased from ~ 5 to 50 Hz (fig.5 B). This increase was also accompanied by a corresponding increase in the average $Gain_R$ in gamma frequency (30-200 Hz) (fig. S4 B). The $Gain_R$ G_{max}, however, increased upto a certain range (50 ms), and decreased thereafter (fig.5 F).

These observations are conforming to the previous findings (Higgs and Spain 2009), whereby the peak frequency of the lower frequency resonance was observed to increase and the resonance strength was observed to decrease with input filtering; which was mostly mediated by the bursts. Our results thus confirm the role of bursts as a mechanism of active gain modulation.

Analysis of the voltage response

The observed parallelism between the subthreshold and suprathreshold signal gain so far and the invariance of the $Gain_R$ to the mean firing rate suggest that under in-vivo like level of activity, the firing rate responses of stellate cells are governed mainly by the dynamics of the underlying subthreshold process, determined by an interplay between the intrinsic frequency selectivity and the synaptic kinetics. To test this further, we did a detailed analysis of the temporal and spectral characteristics of the actual voltage responses.

To begin with, we observed a consistent peak in theta frequency in the power spectrum of the voltage response (V(f)) (fig.6 A Ctrl). The 12 cells used for this analysis were mostly confined to the dorsal region, and within these cells, interestingly, we also observed a weak dorso-

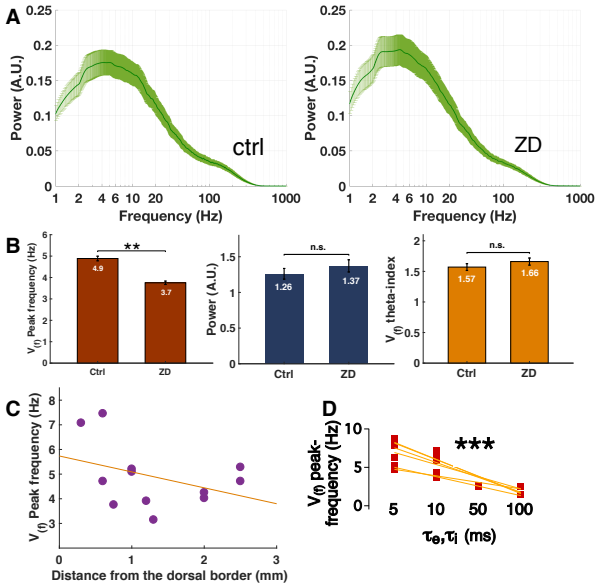

Fig. 6 Analysis of the voltage response

A. Average power spectrum of the voltage response in control (Left) and after blocking HCN channels with ZD7288 (Right). The plots represent average for 12 cells, error bars are SEM. B. Summary of the changes in the the peak frequency (Left), actual power at peak (Middle) and theta-index (Right) in the presence of ZD7288. C. Changes in the peak frequency as a function of D-V distance. D. Changes in the peak frequency as a function of input kinetics.

B: ** $p < 0.01$, Student's paired t-test; n.s. non-significant, C: non-significant, correlation test, D: *** $p < 0.001$, Kruscal-Wallis test.

ventral gradient of the V(f) peak frequency (fig. 6 C).

This can possibly explain the failure of earlier studies perhaps not selective to dorsal region, to observe a similar frequency selectivity while using mimicked synaptic conductances (Fernandez and White 2008).

Next, we observed a small but significant shift in the peak frequency of the power spectrum of the voltage response to lower frequencies when the HCN channels were blocked (fig.6 A, ZD, 6B), suggesting a role of HCN imparted resonance mechanisms. The default synaptic time constants used for analysis were somewhat slower, and the 3 Hz frequency selectivity observed after blocking HCN channels could have emerged from these synaptic kinetics themselves (Nolan et al. 2007). The selectivity to theta frequency with HCN can then result from a faster modulation of these synaptic inputs.

A V(f) peak shift to lower frequencies was also observed when the input kinetics were made slower (fig.6 D), which is intuitive given the

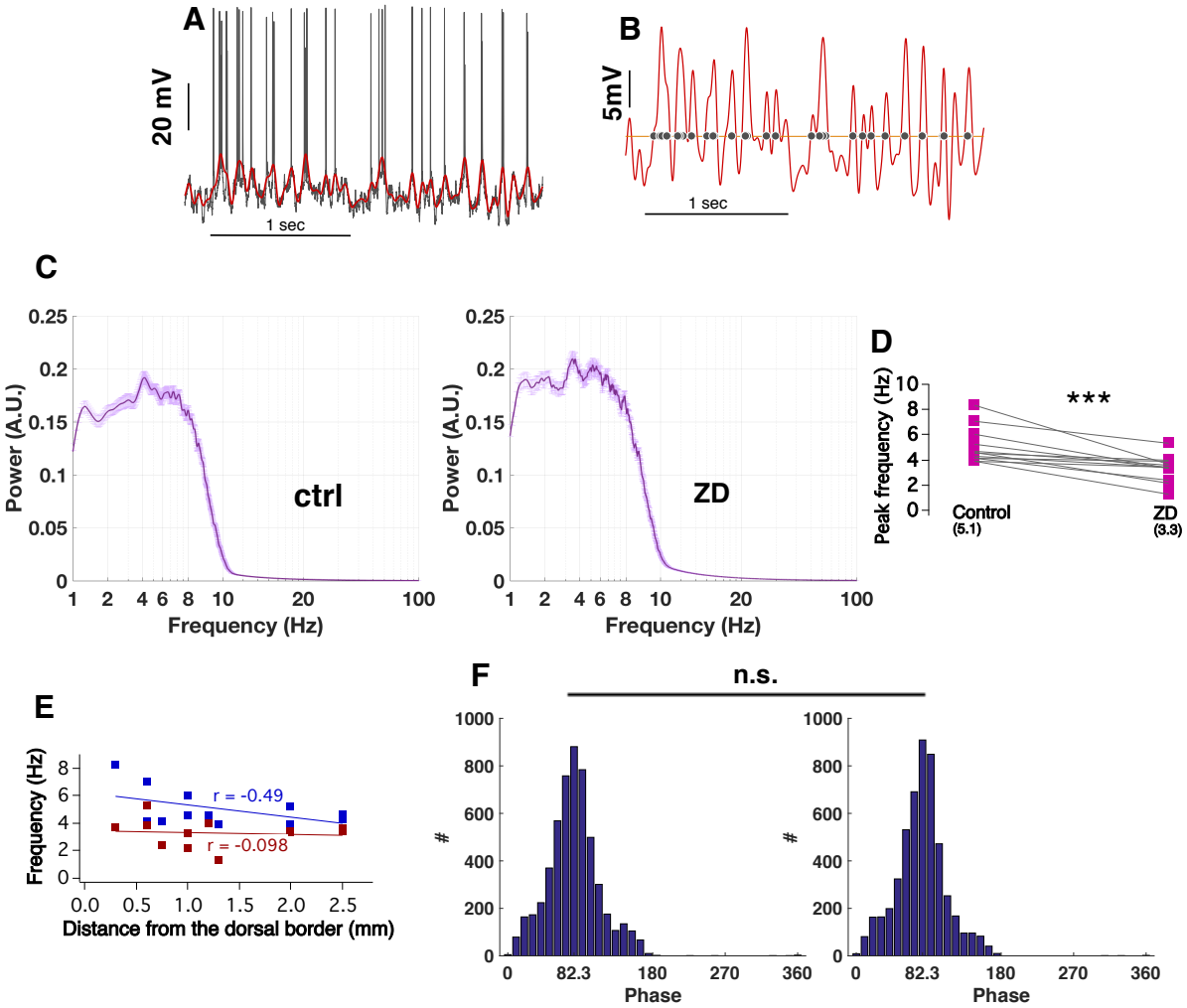

Fig. 7 Theta frequency modulation of synaptic inputs by HCN channels
A. 4-15 Hz band-pass filtered signal (red) overlaid on the actual voltage trace (black). B. The theta signal in A (red), and the corresponding spike timings (grey circles). C. Average power spectrum of the theta response in control (Left) and after blocking HCN channels with ZD7288 (Right). The plots represent average for 12 cells, error bars are SEM. D. Changes in the peak frequency of the theta power spectrum (C), for 12 cells in the presence of ZD7288. E: Changes in the peak frequency of the theta power spectrum (C) as a function of D-V distance for control (blue) and with ZD (red). F. Spike phase histograms for the pooled spike phases of 12 cells corresponding to their theta signals (see methods for the phase assignment).
D: *** $p < 0.001$, Student's paired t-test, E: Individual regression fits: non-significant, correlation test, F: n.s.: difference in the distributions non-significant, Kruscal-Wallis test.

dominance of lower frequencies in voltage response with slower inputs.
The power spectrum of the collective voltage response was thus found to be highly sensitive to multiple factors, suggesting that its consideration as a sole indicator of the actual underlying mechanisms is questionable.

Voltage signal demonstrates a robust theta frequency modulation of synaptic inputs by HCN channels

Next, to probe further the possible theta frequency modulation of synaptic inputs by HCN current, we extracted the underlying theta oscillatory signal (fig.7 A) from the collective voltage response by 4-15 Hz band pass filtering, and analyzed it further.
Prominent rhythmicity in the theta range was observed in this filtered signal, and aligning the spike timings clearly indicated the preference of spikes for the theta peaks (fig.7 B).

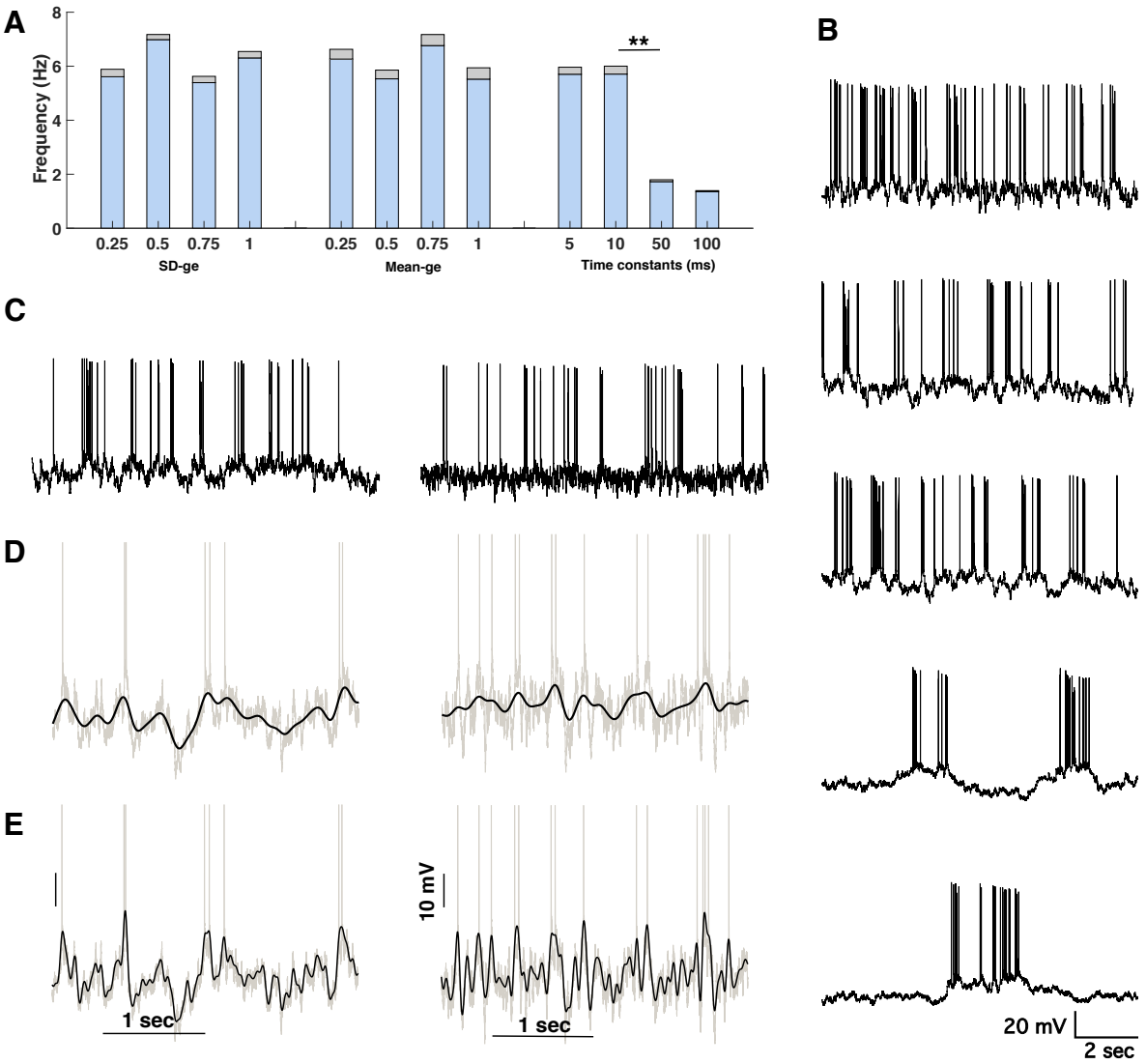

Fig. 8 Theta oscillatory activity is sensitive to the excitatory input kinetics
A. Changes in the peak frequency of the theta power spectrum, as a function of the excitatory strength (normalized SD, mean of the excitatory conductance) and excitatory-inhibitory time constants. B. Voltage traces for the matched excitatory-inhibitory time constants varied from 50 ms, 100 ms, 200 ms, 500 ms, to 1000 ms top to bottom. C. Left: Voltage trace for excitatory time constant = 100 ms, and inhibitory time constant = 10 ms; Right: Vice-a-versa. D. 3 Hz low-pass filtered ramp signal for the traces in C. E: 4-15 Hz band-pass filtered theta signal for the traces in C.
A: ** $p < 0.01$, Student's paired t-test, others: non-significant, Student's paired t-test & Kruscal-Wallis test.

For our moderately slow and E-I matched synaptic time constants, the peak in the power spectrum of this signal was obtained near 5 Hz on average. This peak frequency after blocking HCN channels was significantly reduced (fig. 7 C, D), indicating a salient theta frequency modulation of synaptic inputs by HCN channels. This peak frequency also showed a D-V gradient for the sample size tested, which, interestingly, was flattened in the presence of ZD (fig. 7 E).

Next, in order to determine the extent to which this theta oscillatory activity influences the spike timings, we analyzed the distribution of spike phases over the underlying theta/delta (1.5-4 Hz) signal. We observed that most of the spikes were fired on the near peak ascending phase in control as well as with ZD7288 (mode = 82.3 for 100 bin histogram; fig.7 F), and the distributions of spike phases in both cases were almost identical.

Summarizing, for the given input parameters, HCN channels significantly contribute to the theta frequency modulation of synaptic inputs; the spikes are always preferentially fired on the peaks of this theta signal; but this signal oscillates at a slower pace when the HCN induced resonance mechanisms are absent.

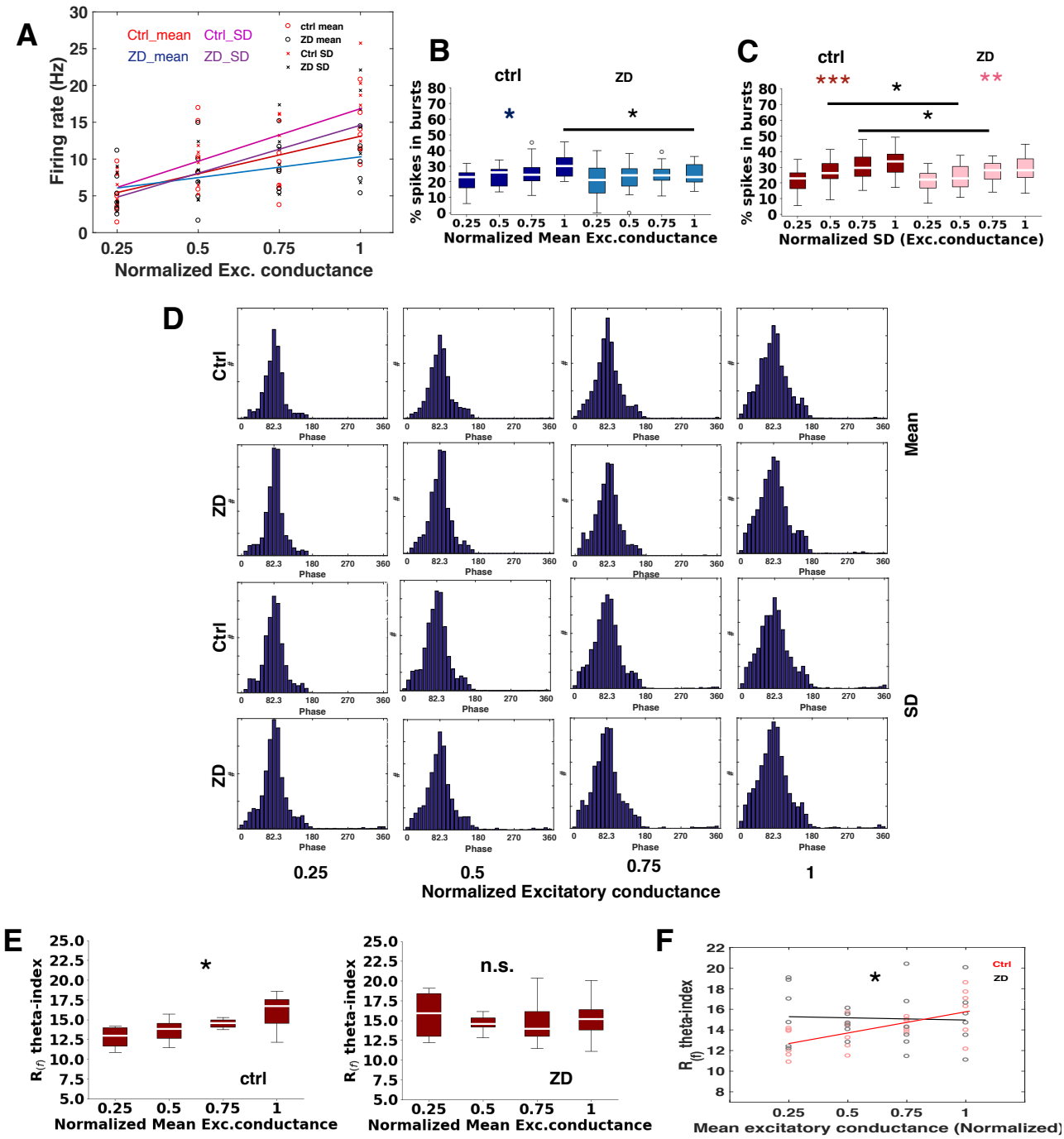

Fig.9 Analysis of the excitation driven firing rate response

A. Mean firing rate as a function of the mean and SD of the excitatory conductance. B,C. Percentage of spikes fired in bursts as a function of the mean and SD of the excitatory conductance in control and with ZD. D. Spike phase histograms showing distribution of spikes over theta cycles, as a function of the mean and SD of the excitatory conductance in control and with ZD.

E. Theta-specific modulation of the firing rate response (theta-index of the rate response power spectrum), in control and with ZD. The overall increase was significant in the control case, but not with ZD. F. One-way analysis of covariance of the data in E shows a significant difference in slopes of excitation driven theta specific firing rate modulation between control and the test case.

B,C. : *** $p < 0.001$, ** $p < 0.01$, * $p < 0.05$, Kruscal-Wallis test for the pooled data, Student's paired t-test for the individual experiments. E: * $p < 0.05$, n.s: non-significant, Kruscal-Wallis test, F. * $p < 0.05$, Analysis of covariance, F-test.

Theta oscillatory activity is sensitive to the excitatory input kinetics

The results so far indicated that under in-vivo conditions, the synaptic inputs can be paced in a preferred frequency range by the neuron's intrinsic resonance mechanisms; and even in the absence of such mechanisms, albeit in lower frequencies, a rhythmicity in the input structure can be present. These findings tally with the previous reports of persistent delta frequency rhythmicity in HCN1 KO mice (Nolan et al. 2007).

To understand the effects of input statistics on the underlying theta rhythmicity, we then analyzed the theta oscillatory signal while systematically varying the input parameters. For the control conditions, no significant change in the frequency of theta signal was observed on varying the SD and mean of the excitatory input as before, and also on varying synaptic kinetics within a certain range. But beyond this range of input kinetics, the frequency dropped significantly beyond the theta band as the input time constants increased (fig.8 A).

At this stage, however, as the input kinetics were becoming slower, the voltage response started exhibiting slow ramp-like motifs, which became more and more prominent on increasing the synaptic time constants (fig.8 B). The increase in time constants was thus accompanied by a decrease in theta rhythm and emergence of slow ramps. It should be considered here that the synaptic kinetics so far were varied similarly for the excitatory and inhibitory inputs, thus making their individual contribution ambiguous. So in a couple of separate cells, we selectively made the excitation or inhibition slower, while keeping the other at the default (which is relatively faster); and observed that the time constants of excitation are the ones to play a crucial role in determining the underlying rhythmic nature. When the inhibition was made faster, the visible ramps could still form (fig.8 C Left); but that was not the case when the excitation was made faster against a slow inhibition (fig.8 C Right); indicating that the emergence of ramps (fig.8 D) requires a predominantly slow excitation. Also, interestingly, the underlying theta signal, became visibly faster as the excitation was switched to the fast mode (fig.8 E), underlining the role of excitatory kinetics in controlling the pace of the fluctuating synaptic activity.

Analysis of the excitation driven firing rate response

Next, in order to determine to what extent this subthreshold theta modulation can influence the suprathreshold responses of these cells, we did a detailed analysis of the temporal and spectral characteristics of the firing rate response. As stated previously, the firing rates increased with an increase in both, the mean and SD of the excitatory conductance, and the initial firing rates for the control and the ZD experiments were comparable (fig.9 A).

We observed however, that the percentage of spikes fired as bursts, increased significantly with increase in the mean excitatory conductance in the control case, but not with ZD (fig. 9 B). With increase in the SD, the bursts increased significantly in both control as well as with ZD, but the average number of bursts were significantly higher in the control case, for the entire middle range of the SDs tested (fig. 9 C).

Next, to understand the relationship of these gamma frequency bursts with the underlying theta signal, we analyzed the distribution of the spikes over the theta/delta phases as before, and observed that, in all the cases most of the spikes were still fired aligned to the peaks, in control as well as with ZD (fig. 9 D).

These findings clearly indicate that in the presence of HCN, there are more number of bursts in response to increasing excitatory drive, which are being modulated in the theta frequency, as opposed to lesser number of bursts with ZD, which are modulated in the slower delta frequencies, thus demonstrating an overall stronger theta-gamma coupling in the presence of HCN.

To confirm this further, we analyzed the actual theta frequency modulation of the firing rate response, and observed that the theta-index of the power spectrum of the rate response increased significantly with the mean excitation in the control case, but not with ZD (fig. 9 E). Further analysis confirmed that the slope of this theta frequency modulation was significantly higher in the control case (fig. 9 F).

Inhibition controls the frequency selectivity in signal gain in the absence of HCN channels: insights from the computational model

In order to verify the mechanistic understandings gathered so far, we constructed a computational

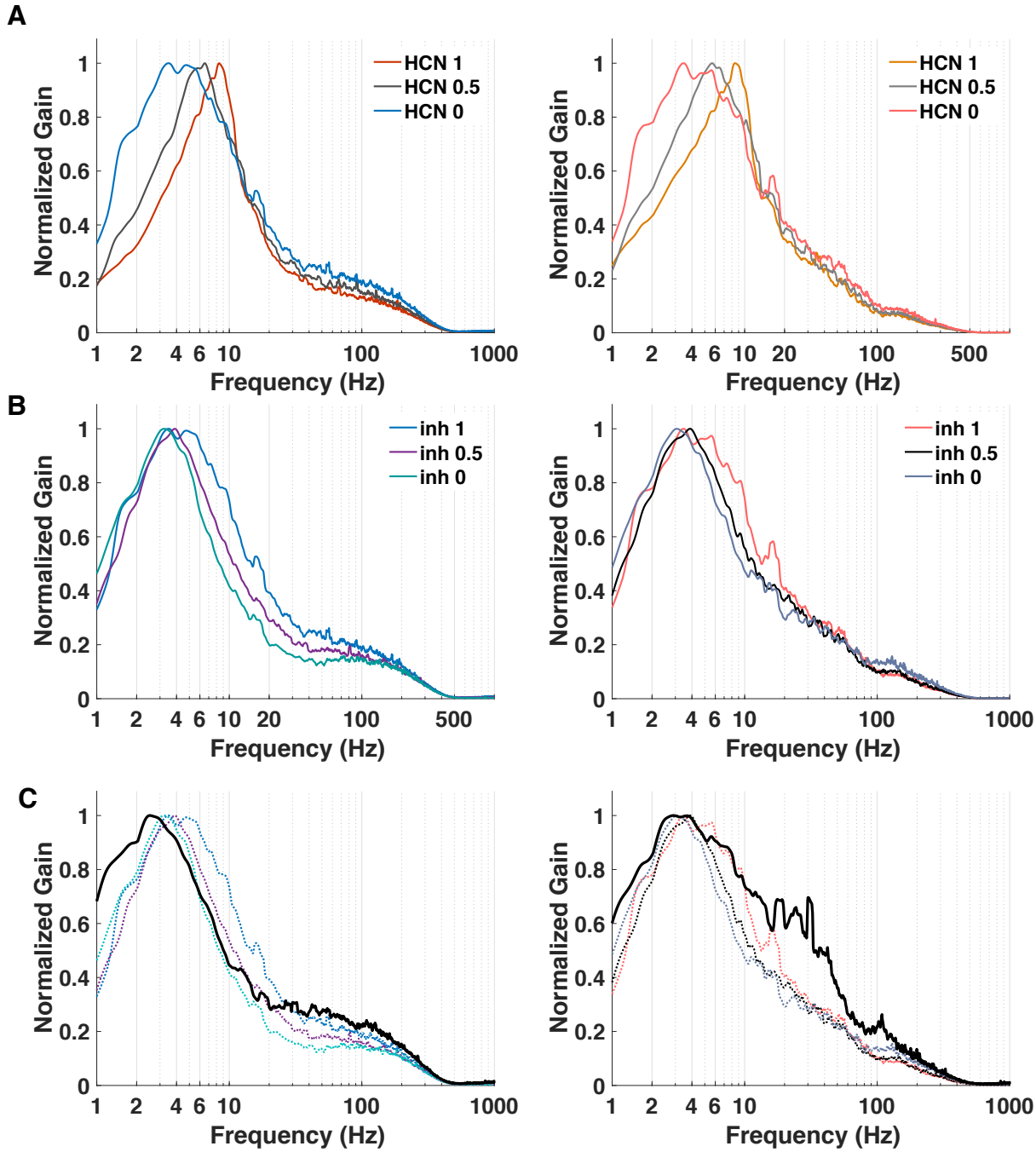

Fig.10 Inhibition controls the frequency selectivity in signal gain in the absence of HCN channels
A. Normalized GainV (Left) and GainR (Right) as a function of normalized HCN conductance. B. Normalized GainV (Left) and GainR (Right) as a function of normalized inhibitory conductance in 0 HCN condition. C. Normalized GainV (Left) and GainR (Right) with excitatory time constant increased from the default 10 ms to 100 ms (black) in 0 HCN, 0 inhibition condition, overlaid on traces in B. The plots in A,B,C represent average of 10 trials of 30 sec. each.

model of MEC Stellate cell, and subjected it to the similar input regime.

The electrophysiological signatures of stellate cells and the hallmarks of successfully operating in-vivo activity could be tallied in the model (fig. S5) enabling us to proceed with the signal gain measurements.

The $Gain_V$ and $Gain_R$ estimated from this model displayed similar theta frequency selectivity as observed experimentally, thus confirming the sufficiency of proposed mechanisms. Now, for a

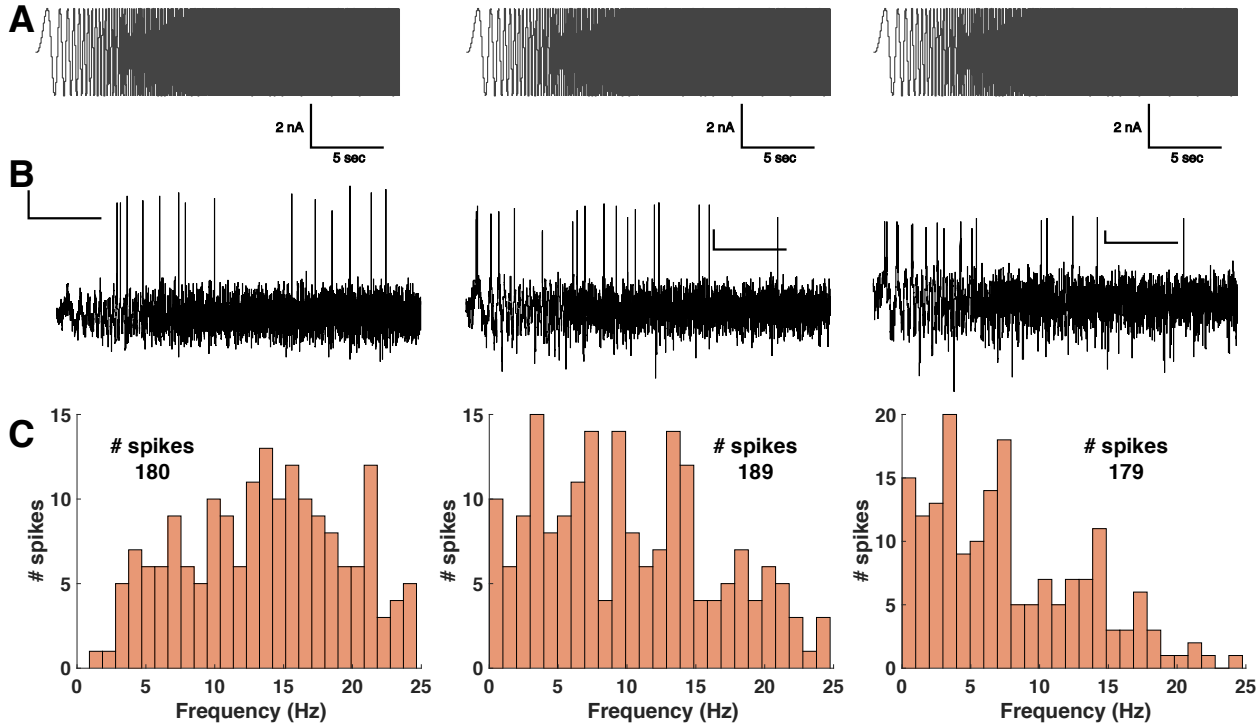

Fig. 11 Firing over slow stimulus frequencies is suppressed by HCN and inhibition
A. 25 sec. long chirp stimuli spanning 25 Hz in 25 sec. B. Voltage responses to stimuli in A injected under the in-vivo regime, for control (Left), no HCN (Middle), and no HCN-no Inhibition (Right). Scale Bar: 5 sec., 20. mV in all panels. C. Histogram of spike times for total spikes fired in 10 trials as a function of stimulus frequency, for data in B.

better substantiation of the role of HCN channels, we decreased the HCN conductance in two steps, and observed a likewise shift of gain peak to lower frequencies, and a decrease in theta-index for both $Gain_V$ and $Gain_R$ (fig.10, A). The experimentally observed theta-modulation by HCN channels could also be verified in the computational model (fig. S6).

Further, in an attempt to understand which factors can dictate the remaining frequency selectivity in the absence of HCN channels, we decreased the strength of inhibition in two steps, and observed the frequency preference to shift further left (fig.10, B). Considering that a gradient of grid cell periodicity remains in the absence of HCN channels (Giocomo et al. 2011), and a dorsoventral gradient of inhibition is present in MEC (Beed et al. 2013), these observations should be noteworthy.

The analysis so far was carried out at the default synaptic time constants, and a possibility remained that after removing HCN channels and inhibition, excitation can further affect the signal gain. So, we re-did the analysis using substantially slow excitation and observed that the remaining small frequency selectivity is noticeably affected by the slower excitation (fig.10 C) for $Gain_V$ as well as for $Gain_R$. The gamma frequency gain for $gain_R$ was also visibly increased following the change in excitatory kinetics (fig.10 C Right), corroborating the experimental findings of such increase with slower input time constants (fig. S4, B).

Theta frequency selectivity in signal gain correlates with reduced firing over the lower input frequencies

Finally, to directly verify the effects of input selectivity analyzed so far, we tested the model with chirp stimuli (fig. 11 A), with stimulus frequency adjusted to increases from 0 to 25 Hz in 25 sec.

The roles of HCN channels were evident from the lesser firing on lower frequencies in the presence of HCN (fig.11 B,C Left), which increased after the HCN channels were removed (fig.11 B,C Middle). Further, after removing inhibition from the cell, the firing over lower frequencies was observed to increase even more (fig.11 B,C

Right), thus underlining the ability of inhibition in imparting weak resonance mechanisms to the neurons in the absence of HCN channels.
The results so far suggest that the underlying HCN-based resonance mechanisms in stellate cells manifest in the modulation of voltage responses in theta frequency and also bias the preference of these voltage responses for the theta-frequencies in the stimulus. Collectively, HCN current and inhibition thus reduce firing both on and in lower frequencies.

Methods

Brain slice preparation
The guidelines of 'Animal Ethics and Welfare Committee' of the Indian Institute of Science, Bangalore, India were followed in all the experiments. 5-8 week old male SD rats (weighing ~130 - 250 g) were used in the study.
Rats were anesthetized by intra-peritoneal injection of a combination of Ketamine and Xylazine (dose calculated according to the animal weight). After onset of deep anaesthesia, as determined by cessation of toe-pinch reflex, rats were transcardially perfused with ice-cold cutting solution (see Solution composition) continuously bubbled with carbogen (a mixture of 95% O_2 and 5% CO_2 gas), and then decapitated. During dissection, the skull was carefully separated through its midline and the brain was scooped out using a blunt spatula from the side of the cerebellum and was immediately transferred to sACSF (see Solution composition) pre-chilled to 0-4 ºC and continuously bubbled with carbogen. This part of the dissection was usually completed within a minute.
Parasagittal hippocampal slices (350 mm) were then obtained according to the guidelines provided by previous reports (Pastoll, White, and Nolan 2012), while submerged in oxygenated ice-cold cutting solution, using Leica VT1000S vibratome. Brain slices were then transferred to the incubation solution (see Solution composition) in an incubation chamber, maintained at 34 ºC using a water-bath. Slices were placed according to the hemisphere maintaining the order in which they were obtained. The incubation solution was pre-bubbled with carbogen which was continued throughout the incubation period.
After 15 minutes of incubation, the incubation chamber was transferred to room temperature (~ 24 ºC), continuing the carbogen bubbling. Electrophysiology recordings were started after 1-hour recovery period from the end of this incubation.

Solution composition:
The following solutions were used for the electrophysiology experiments.
(all salts from Sigma Aldrich).
Sucrose based Artificial Cerebrospinal Fluid (sACSF):
The solution used for acute slicing procedure contained (in mM): Sucrose (230), KCl (2.5), $MgCl_2.6H_2O$ (7), $CaCl_2.2H_2O$ (0.5), $NaHCO_3$ (25), NaH_2PO_4 (1.25), Glucose (10), Sodium Pyruvate (3). pH 7.4, osmolarity ~ 290 – 330 milliosmoles.
Incubation Solution:
The slices were incubated in an incubation solution containing (in mM): NaCl (125), KCl (2.5), $MgCl_2.6H_2O$ (2), $CaCl_2.2H_2O$ (2), $NaHCO_3$ (26), NaH_2PO_4 (1.25), Glucose (25), Ascorbic acid (1), Sodium Pyruvate (2). pH 7.4, osmolarity ~ 290 – 310 milliosmoles.
Artificial CerebroSpinal Fluid (nACSF):
For electrophysiology recordings, the slices were transferred to the nACSF containing (in mM): NaCl (125), KCl (3), $MgCl_2.6H_2O$ (1), $CaCl_2.2H_2O$ (2), $NaHCO_3$ (25), NaH_2PO_4 (1.25), and Glucose (10); pH 7.4; osmolarity ~ 290 – 310 milliosmoles.
Internal Solution:
The patch pipettes were back filled with an internal solution consisting of (in mM):
Potassium gluconate (120), KCl (20), HEPES (10), Disodium phosphocreatine (10), MgATP (5), Na_2GTP (0.5), EGTA (0.2). pH 7.4; Osmolarity: ~ 290 – 310 milliosmoles.

Pharmacological agents:
During experiments, these were perfused with nACSF when required.
Synaptic Blockers:
CNQX 10 µM, (+)bicuculline 10 µM, picrotoxin 10 µM, D,L-AP5 50 µM, CGP55845 5 µM (Abcam).
HCN blocker:
ZD7288 25 µM (Tocris Bioscience).

Data acquisition and analyses:

Experiments were performed in nACSF at 34 ºC; maintained with the help of a bath chamber heater connected to an automatic temperature controller (Harvard Apparatus, USA). The patch pipettes (1.5 mm O.D., 0.86 mm I.D.) were prepared using P-97 puller (Sutter Instruments, USA) and fire polished to achieve a final access resistance of 3.5 - 5 MΩ. These were then back filled for stellate cell recordings, with the internal solution.

Medial Entorhinal cortex layer II stellate cells were identified using infrared Dodt gradient contrast video microscopy (Olympus BX51WI). These putative stellate cells were then patched in whole-cell current-clamp configuration to record intrinsic electrophysiological properties and their modulation.

Somatic whole cell recordings in fast current-clamp mode were performed using DAGAN-BVC 700A amplifier, (Dagan Corporation, USA), Digidata 1440A Digitizer (Molecular Devices, USA), and WinWCP software package (Strathclyde Electrophysiology Software, UK). The signals were filtered at 5 kHz and stored on disk at > 20 kHz sampling frequency. Series resistance (< 25 MΩ) was fully compensated in the current clamp mode. Series resistance was monitored and compensated online using the bridge-balance circuit of the amplifier.

The following parameters i.e., resting membrane potential (RMP), input resistance (R_{in}) and series resistance (R_s) were regularly monitored during the electrophysiological recordings. Recordings in which the series resistance did not change > 5 MΩ throughout the duration of the experiment were included for analysis. The stellate cells had their break-in RMP of ~ -62 - -65 mV. Unless otherwise stated, experiments were performed at the initial resting membrane potential of the cell. Cells showing RMP depolarized than -60 mV during the recordings were discarded from the analyses.

The system for the dynamic clamp experiments consisted of the Real-time Experiment Interface (RTXI) (version 2.0-rc3, http://www.rtxi.org/) installed on a personal computer, Dagan BVC 700A amplifier and PCI-6221 multi-function data acquisition (DAQ) board (National Instruments, USA), with a BNC-2090A coaxial cable interface. Dynamic clamp signals were filtered at 5 kHz and sampled at 10 kHz.

Mimicking in-vivo states

After recording the basic neuronal parameters in current clamp, the recording mode was switched to the dynamic clamp.

The fluctuating synaptic conductance (Gfluct) module in the dynamic clamp (adapted from (A. Destexhe et al. 2001) and Gfluct.mod file (ModelDB Accession: 8115)), was used to generate in-vivo like background synaptic activity.

The Default Gfluct parameters

The mean excitatory conductance: g_e0 = 0.03 μS, The mean inhibitory conductance: g_i0 = 0.06 μS, Standard deviation of the excitatory conductance: std_e = 0.01 μS, Standard deviation of the inhibitory conductance: std_i = 0.02 μS, Time constant for the excitatory conductances: Tau_e = 10 ms, Time constant for the inhibitory conductances: Tau_i = 10 ms,
Excitatory reversal potential: e_rev = 0 mV, Inhibitory reversal potential: i_rev = -75 mV.

The voltage responses and the applied current were recorded for 8-10 trials of ~10 sec. each.

This duration was increased when the slower synaptic conductances were used, to account for the slower firing rate and to sample approximately the same number of spikes.

The changes in basic electrophysiological properties were monitored periodically. The changes in series resistance were monitored and adjusted for in between the trials.

Experiments to test the role of input statistics

In a set of experiments designed to test the effects of varying mean and SD of excitation,
the SD of the excitatory conductance was varied from 0.002 μS to 0.02 μS in steps of ~0.005 μS, while holding the mean unchanged at the default value. Then, the mean of the excitatory conductance was varied from 0.02 μS to 0.04 μS in steps of 0.005 μS, while holding the SD unchanged at the default value.

To test the role of synaptic kinetics, the time constants of excitatory and inhibitory synapses were changed from 3-5 ms, 10 ms, 50 ms, 100 ms and 200 ms; keeping rest of the parameters default. These values are selected considering the time constants of the synapses observed in-vivo, and those used previously for the stellate

cells (A. Destexhe et al. 2001; Fernandez and White 2008).
In a small subset of experiments, extreme values of synaptic time constants such as ~ 0 or 500 – 1000 ms were used to confirm the mechanistic interpretations.

Experiments to test the role of I_h
To test the role of HCN current, ZD7288 was used as HCN channel blocker.
After recording all the control traces, 25 μM of ZD7288 was bath perfused. The test recordings were started ~ 10 min. after starting this perfusion, and after ensuring a complete HCN block via the electrophysiological signatures.

Data Analyses
Acquired electrophysiological data were analyzed using Igor Pro 6 (Wave Matrix, USA), Matlab (The MathWorks, Inc.), Python programming language (Python Software Foundation), and Clampfit (Molecular Devices, USA).
The input resistance was measured at the steady state of voltage deflection.

Estimation of signal gain
The neuronal voltage response was analysed in two different ways to estimate the signal gain.
In the first case, the collective voltage trace was analysed in the time and frequency domain.
For the further analysis, however, a vector of smoothly varying instantaneous firing rate as a function of time was constructed from the actual voltage response.
To calculate the signal gain, a ratio of the Fourier transform of the response and the Fourier transform of the stimulus (applied current) was calculated (Analysis done in Matlab). The gain function thus obtained was filtered using a Gaussian window and smoothened using a moving average. The window width was adjusted so as to achieve a noise free trace, without compromising on the signal information. On average, a window of 20 X-axis data points was used, corresponding to ~ 1.5 Hz.

Analysis of underlying theta oscillations and slow synaptic ramps
To compare the changes selective to the theta frequency range, the output voltage traces were band-pass filtered using a 4-15 Hz FIR filter. Similarly, to analyze the slowly varying ramps, the output voltage traces were low-pass filtered using a 3 Hz FIR filter.

Estimation of spike phases
For estimating the distribution of spike phases, the theta and ramp signals were used to determine their peak times (corresponding to the positive peak), trough times (corresponding to the negative peak), and zero-times (all time points where the signal crosses zero: The mean of the mean subtracted, normalized signal).
Thus, three zero-points constituted one oscillatory cycle. Phases from 0-360 were then assigned to each cycle. A phase vector corresponding to the original voltage trace could be thus obtained, which allowed to compute the phase corresponding to each particular spike.
The mean, median, mode and variance of spike phases were then computed from a histogram of pulled spike phase values.

Analysis of bursts
To study the percentage of spikes occurring as bursts, spikes occurring in 50-100 Hz bursts were considered as a single spike, and spike time of only the first spike in the burst was considered. The number of spikes and the firing rate was then recalculated.

Computational model
A single compartment model of MEC layer-II stellate cell was built in NEURON simulation environment (Hines and Carnevale, 1997), with parameters adjusted to match the observed electrophysiological responses of the Stellate cells.

Fluctuating conductances
The in-vivo like fluctuating synapses were modelled according to the Gfuct.mod input regime already discussed under “Mimicking in-vivo states”.

Voltage gated Na^+ and K^+ channels
Adapted from a computational model by Destexhe et. al., 2001.
ModelDB Accession:8115
HCN channels
Adapted from (Christoph Schmidt-Hieber and Häusser 2013).
ModelDB Accession:150239

Persistent Na^+ channels
By (Uebachs et al. 2010).
Assumes a non-inactivating conductance.
ModelDB Accession:125152
K_{AHP} channels
Adapted from (Migliore et al. 1995)
ModelDB Accession: 3263.
L-type Ca^{++} channels
Voltage gated high threshold activated calcium channel, adapted from (Migliore et al. 2006).
ModelDB Accession: 64229
Calcium handling mechanism
Models the decay of the internal calcium concentration due to calcium currents and pumps.
Adapted from (A. Destexhe et al. 1996).
ModelDB Accession: 17663

Statistical Analysis
The tests used for hypothesis testing and calculating the p-values are described with the individual results.
Typically, student's paired t-test, Kruscal-Wallis test, Analysis of covariance (ANCOVA), and F-statistics were used as appropriate.
The statistical analysis was carried out using Matlab, MS-Excel and the Python programming language.

Discussion

Signal gain, resonance and input statistics:
Neuronal representations, the activity patterns which correspond to the features of the outside world, emerge through a clever processing of information, presented to them through a noisy synaptic bombardment of around 1000-10000 inputs arriving simultaneously. Under these in-vivo high conductance states, the membrane resistance is significantly low and the assumptions of linearity are questionable (Chance, Abbott, and Reyes 2002; Alain Destexhe, Rudolph, and Paré 2003). Neuronal computations under these conditions thus rely on amplifying a certain frequency signals (Higgs and Spain 2009), and can be better analyzed by studying the impedance, which is a frequency-domain extension of the concept of resistance (Hutcheon and Yarom 2000).
In-vitro impedance amplitude profile in stellate cells has already confirmed their theta-range resonance frequency, which owing to the intrinsic amplifying mechanisms, also reflects in their subthreshold oscillations. Many theories of grid pattern formation rely on a gain factor dictating the increase in the frequency of these oscillations in response to the speed modulated excitatory drive (Burgess 2008; Bush and Burgess 2014; Jeewajee et al. 2008), leading to an interference pattern, which can generate periodic firing fields. This gain factor is thus thought to dictate the grid spacing in these models. However, oscillations in-vivo were found to be not strong enough to generate firing fields, which could form independent of them through the synaptic ramps (Domnisoru, Kinkhabwala, and Tank 2013). So the question of which alternate mechanisms are operational to decree the grid spacing remains.
The necessity of HCN1 channels for maintaining the grid spacing was confirmed by the experiments on the HCN1 KO mice (Giocomo et al. 2011). Thus, although the in-vivo theta oscillations are not strong enough to generate the grid fields, it becomes interesting to see whether they are a reflection of the underlying HCN influenced resonance mechanisms, and whether this resonance expresses itself in any other way in the modulation of the stellate cell voltage responses.

Resonance still operates in presence of noise at subthreshold scale, and can influence firing rate response
In this light, we tested the frequency dependent gain in stellate cells of the MEC, subjected to in-vivo like high conductance bombardment generated through the dynamic clamp; and observed that HCN channels play a major role in confining the signal gain to theta-frequency even in the presence of strong noise. This theta-frequency selectivity in gain was observed for both the subthreshold responses and the rate modulation.
Thus, the HCN mediated resonance mechanisms are still active during the in-vivo states, in spite of a drastic drop in input resistance and high noise levels.
Another major role attributed to HCN channels is their effect on membrane resistance, which determines membrane time constant, and which in turn, affects the neuronal integrative properties. However, under in-vivo states, where the membrane resistance has already dropped

by ~ 70-80%, the reciprocal effects of HCN conductance have been questioned (Mishra and Narayanan 2014). These effects should have reflected in the actual amplitude of $Gain_V$. Such increase was indeed observed, but the theta specific $Gain_V$, theta-index, was rather found to decrease in the absence of HCN channels. Thus, although the effects of increased membrane resistance with ZD increase the overall gain, HCN channels can modulate the gain in a frequency dependent way, by selectively increasing the gain over theta frequencies.

Sensitivity of signal gain to the latent noise statistics

Next, as we systematically perturbed the input noise statistics, we observed that although the gain amplitude was sensitive to the input strength, its frequency selectivity was unaffected by such input scaling.

Interestingly, the gain amplitude was observed to respond differentially to the mean-driven Vs. the fluctuation driven increase in the excitatory conductance; possibly owing to the effects of the underlying inward HCN current. In control conditions, it decreased with the depolarization caused by an increase in SD of excitatory conductance. This was possibly a result of deactivation of the HCN inward current, which, owing to its high-pass filtering properties, selectively increases the gain of the fluctuating inputs. Ratifying this, such an increase was not observed with ZD (where the HCN channels are already deactivated), and with increase in mean excitation (where although the inward HCN current deactivates with depolarization, the direct increase in the mean excitation is able to balance out these effects).

On making the synaptic kinetics slower, we observed a small but significant rightward shift in the otherwise unperturbed theta frequency peak, and an increase in the average gamma frequency gain. Both these findings corroborate the earlier reports of stronger higher frequency resonance when these frequencies in the input are weaker (Higgs and Spain 2009). These mechanisms through which the neurons can amplify the weaker but important latent signals; reported in other brain regions, with current based inputs (Higgs and Spain 2009); are thus also active in the MEC stellate cells, under the high, conductance based noise.

This differential responsiveness of gain to the mean, SD and kinetics of stimulus can be a dynamic gain control mechanism, wherein the neuronal sensitivity to the input statistics is enhanced, enabling a state-dependent adaptation of their responses.

Thus, rather than being dampened by noise, we rather observed the resonance to emerge through the latent noise statistics.

Resonance in signal gain manifests in the theta modulation of synaptic inputs

Next, we did a detailed analysis of the temporal and spectral characteristics of the actual voltage responses, to detect the signatures of the functioning resonance mechanisms. We observed a theta range spectral selectivity in the power spectrum of the voltage responses, which was sensitive to HCN channels, and which could also be influenced by the synaptic kinetics.

Collective voltage response can thus be a reflection of multitude of underlying processes, where the same response can be achieved through a combination of underlying players, according to the neuronal and network state; and should not be considered as a sole indicator of the actual underlying mechanisms.

Next, in order to test whether the theta resonance mechanisms evident from the signal gain can influence the subthreshold dynamics of the synaptic inputs, we extracted and analyzed the underlying theta signal, and found it to be indeed potent in modulating the synaptic inputs in theta frequency.

An analysis of spike phases confirmed that the spikes are always fired selectively near the peak of this signal, suggesting the possible influences on the firing rate modulation. Next, in the presence of ZD, the frequency of this signal dropped to the delta range, but the spikes were observed to be still fired selectively near the peak.

On studying the effect of input statistics on this theta modulation, we observed that the frequency of the underlying theta signal in control case was unaffected by the excitatory drive, but was sensitive to the excitatory input kinetics; which when faster could contribute to the theta modulation, but when slower, mostly transformed into ramp-like motifs.

Thus, an oscillatory activity is still present in the stellate cell voltage responses and is potent enough to modulate the spike timings, notwithstanding the heavy noise. The frequency of this modulation can vary from dorsal to ventral MEC, aligned to the HCN conductance, and it can be suspected that it can have a role in influencing grid-like responses of stellate cells as speculated earlier for the intrinsic oscillations.

Resonance makes theta-gamma coupling robust and affects the slope of excitation-driven suprathreshold theta frequency modulation

Further detailed analysis of the firing rate response suggested the influence of underlying theta signal in controlling its theta frequency modulation. The slope of this theta frequency modulation of firing rate with the mean excitation was significantly higher in the control case where the underlying activity is theta-paced, than with ZD where it oscillates in the delta frequency. Also, it became evident from the analysis of bursts and that of spike phases, that there exists also a corresponding theta modulation of the gamma frequency bursts, which makes the overall theta-gamma coupling stronger in the presence of HCN channels. These findings parallel the similar higher slope of theta frequency modulation by running speed in control mice compared to the HCN1 KO mice (Giocomo et al. 2011), and are also in tune with the previous reports which pointed out the efficacy of the subthreshold resonance mechanisms to attune the firing rate responses in the presence of noise (Brunel, Hakim, and Richardson 2003; Richardson, Brunel, and Hakim 2003).

Input integration and modulation

The HCN driven mechanisms considered previously to be able to control stellate cell voltage responses were mainly the subthreshold oscillations and the input integration. Although the roles of these mechanisms are questionable under in-vivo states for valid reasons (Fernandez and White 2008; Mishra and Narayanan 2014), we observed that the same in-vivo states rather facilitate their expression. The resonance expresses in the theta modulation of inputs, and the theta-coupled gamma frequency responses can be a possible reflection of the reminiscent conductance based effects of HCN leading to narrow coincidence detection window owing to altered spike initiation dynamics (Das and Narayanan 2015).

Also, depending on the differential input integration, we observed emergence of slow ramps with the slow excitatory kinetics and stronger theta modulation with faster excitatory kinetics. Thus, our results bring to surface the key targets: excitatory kinetics and resulting integration, which when affected, can directly influence the synaptic ramp formation and theta-gamma response dynamics.

Possible effects on the grid spacing

We observed the theta-peak of signal gain to be robust to an array of input statistics, and a direct reflection of the strength of HCN conductance. Thus, there is room for speculating that the dorso-ventral gradient of grid spacing is actually a manifestation of the dorso-ventral HCN influenced differential resonance frequencies of the signal gain, which can reflect in the correspondingly faster theta-gamma modulation of the firing rate with the velocity mediated excitatory drive.

Also, our findings of stronger theta modulation with the faster excitatory inputs, and prominent ramps with slower excitatory inputs; considered along with the actual observed presence of both of these in vivo (Domnisoru, Kinkhabwala, and Tank 2013); suggest that two (or more) such distinct excitatory streams with disparate synaptic kinetics should be present in vivo, to justify the observed simultaneous presence of the ramps and the theta oscillations.

And if there are latent signals present in the inputs in the form of proportion of faster to slower kinetics, those too can be decoded under the proposed schema.

Alternate resonance mechanisms:

The reminiscent delta frequency selectivity in signal gain after blocking HCN channels parallels the HCN1 independent perithreshold activity (Nolan et al. 2007) and the reminiscent gradient of grid periodicity observed in the HCN1 KO mice (Giocomo et al. 2011), and indicates a strong possibility of existence of alternate, HCN independent/co-dependent resonance mechanisms. Given that resonance is known to emerge through the interaction of two

counteracting mechanisms (Hutcheon and Yarom 2000), intuitively, in the absence of HCN channels, inhibition is the next suitable candidate. So after confirming the experimentally observed contributions of HCN channels to signal gain in a computational model, we decreased the inhibitory conductance in two steps in the absence of HCN, to check the possible effects of inhibition on the reminiscent frequency selectivity. A leftward shift of signal gain peak was indeed observed, indicating that the reported dorso-ventral inhibitory gradient (Beed et al. 2013) can contribute to the similar gradient of frequency selectivity along the MEC D-V axis, and can underlie the reminiscent gradient of grid periodicity observed in the HCN1 KO mice.

These proposed roles of inhibition are in accordance with those already known in the case of cortical circuits (Stark et al. 2013).

Also, in the same model, the effects of excitatory kinetics in the absence of inhibition further confirmed that weak resonance mechanisms can emerge also through the rhythmic self-modulation of faster excitatory inputs, and if the excitatory kinetics or their post-synaptic manifestations differ along the dorso-ventral MEC axis, they can further contribute to the grid spatial period.

The combined effects of the excitatory-inhibitory dynamics discussed above, can dictate different symmetry breaking operations along the dorso-ventral MEC axis, which can be further fine-tuned by HCN channels, thus setting the grid scale.

The alternate resonance mechanisms can also explain the spatial periodicity observed in the pyramidal cells, where the HCN conductance is not very strong. Another possible and noteworthy resonance phenomenon that can exist in pyramidal cells is the one where the resonance is observed at the the mean firing rate itself, as previously suggested to exist based on the tuning of the noise levels (Richardson, Brunel, and Hakim 2003).

Other implications:

The robustness of stellate cell resonance to noise level can possibly actually be an error-correction mechanism, necessary for maintaining the accuracy of the spatial coding (Sreenivasan and Fiete 2011). A possibility thus also remains that the strong HCN dependent resonance mechanisms in stellate cells, which are also reflected in the firing rate modulation, can influence the network level input statistics (Sinha and Narayanan 2015), thus influencing/generating input statistics based resonance in other cell types (in MEC as well as stellate cell's downstream targets in the hippocampus). Stellate cells in that case can indirectly serve their long believed role of pacemakers.

References

Barry, Caswell, Daniel Bush, John O'Keefe, and Neil Burgess. 2012. "Models of Grid Cells and Theta Oscillations." *Nature* 488(2011): E1–E1.

Beed, Prateep et al. 2013. "Inhibitory Gradient along the Dorsoventral Axis in the Medial Entorhinal Cortex." *Neuron* 79(6): 1197–1207.

Boccara, Charlotte N et al. 2010. "Grid Cells in Pre- and Parasubiculum." *Nature Neuroscience* 13(8): 987–94. http://www.nature.com/doifinder/10.1038/nn.2602.

Brun, Vegard Heimly et al. 2008. "Progressive Increase in Grid Scale from Dorsal to Ventral Medial Entorhinal Cortex." *Hippocampus* 18(12): 1200–1212.

Brunel, Nicolas, Frances S. Chance, Nicolas Fourcaud, and L. F. Abbott. 2001. "Effects of Synaptic Noise and Filtering on the Frequency Response of Spiking Neurons." *Physical Review Letters* 86(10): 2186–89.

Brunel, Nicolas, Vincent Hakim, and Magnus J. E. Richardson. 2003. "Firing-Rate Resonance in a Generalized Integrate-and-Fire Neuron with Subthreshold Resonance." *Physical Review E* 67(5): 51916. https://link.aps.org/doi/10.1103/PhysRevE.67.051916.

Burgess, Neil. 2008. "Grid Cells and Theta as Oscillatory Interference: Theory and Predictions." *Hippocampus* 18(12): 1157–74. http://www.pubmedcentral.nih.gov/articlerender.fcgi?artid=3196519&tool=pmcentrez&rendertype=abstract (July 16, 2014).

Burgess, Neil, C Barry, and J O Keefe. 2007. "An Oscillatory Interference Model of Grid Cell Firing." *Hippocampus* 17(9): 801–12.

Bush, D, and N Burgess. 2014. “A Hybrid Oscillatory Interference/continuous Attractor Network Model of Grid Cell Firing.” *J Neurosci* 34(14): 5065–79. http://www.ncbi.nlm.nih.gov/pubmed/24695724%5Cnhttp://www.ncbi.nlm.nih.gov/pmc/articles/PMC3972729/pdf/zns5065.pdf.

Chance, Frances S, L F Abbott, and Alex D Reyes. 2002. “Gain Modulation from Background Synaptic Input.” *Neuron* 35(4): 773–82. http://www.ncbi.nlm.nih.gov/pubmed/12194875 (February 27, 2018).

Couey, Jonathan J. et al. 2013. “Recurrent Inhibitory Circuitry as a Mechanism for Grid Formation.” *Nature Neuroscience* 16(3): 318–24. http://dx.doi.org/10.1038/nn.3310.

Das, Anindita, and Rishikesh Narayanan. 2015. “Active Dendrites Mediate Stratified Gamma-Range Coincidence Detection in Hippocampal Model Neurons.” *The Journal of physiology* 593(16): 3549–76.

Destexhe, A et al. 1996. “In Vivo, in Vitro, and Computational Analysis of Dendritic Calcium Currents in Thalamic Reticular Neurons.” *The Journal of neuroscience : the official journal of the Society for Neuroscience* 16(1): 169–85. http://www.ncbi.nlm.nih.gov/pubmed/8613783 (July 8, 2018).

Destexhe, A, M Rudolph, T J Sejnowski, and La Jolla. 2001. “FLUCTUATING SYNAPTIC CONDUCTANCES RECREATE IN VIVO - LIKE ACTIVITY IN NEOCORTICAL NEURONS.” *Neuroscience* 107(1): 13–24. http://www.sciencedirect.com/science/article/pii/S030645220100344X.

Destexhe, Alain, Michael Rudolph, and Denis Paré. 2003. “The High-Conductance State of Neocortical Neurons in Vivo.” *Nature Review Neuroscience* 4(September): 739–51.

Dickson, Clayton T. et al. 2000. “Properties and Role of Ih in the Pacing of Subthreshold Oscillations in Entorhinal Cortex Layer II Neurons.” *J Neurophysiol* 83(5): 2562–79. http://jn.physiology.org/content/83/5/2562.short (April 16, 2015).

Domnisoru, Cristina, Amina A. Kinkhabwala, and David W. Tank. 2013. “Membrane Potential Dynamics of Grid Cells.” *Nature* 495(7440): 199–204. http://www.nature.com/doifinder/10.1038/nature11973.

Fernandez, F. R., and J. A. White. 2008. “Artificial Synaptic Conductances Reduce Subthreshold Oscillations and Periodic Firing in Stellate Cells of the Entorhinal Cortex.” *Journal of Neuroscience* 28(14): 3790–3803. http://www.jneurosci.org/cgi/doi/10.1523/JNEUROSCI.5658-07.2008.

Ferrante, Michele et al. “Post-Inhibitory Rebound Spikes in Rat Medial Entorhinal Layer II / III Principal Cells : In-Vivo , In-Vitro Evidence for a Model of Grid Cells Generation PIRS in mEC LII Stellate and LII / III Pyramidal Cell Populations Stimulus Features mEC Dorsal-Ventra.” : 94263.

Garden, Derek L F et al. 2008. “Tuning of Synaptic Integration in the Medial Entorhinal Cortex to the Organization of Grid Cell Firing Fields.” *Neuron* 60(5): 875–89.

Giocomo, Lisa M. et al. 2011. “Grid Cells Use HCN1 Channels for Spatial Scaling.” *Cell* 147(5): 1159–70. http://dx.doi.org/10.1016/j.cell.2011.08.051.

Giocomo, Lisa M, and Michael E Hasselmo. 2008. “Time Constants of H Current in Layer Ii Stellate Cells Differ along the Dorsal to Ventral Axis of Medial Entorhinal Cortex.” *The Journal of neuroscience : the official journal of the Society for Neuroscience* 28(38): 9414–25. http://www.pubmedcentral.nih.gov/articlerender.fcgi?artid=2990529&tool=pmcentrez&rendertype=abstract (July 13, 2014).

Giocomo, Lisa M, Eric a Zilli, Erik Fransén, and Michael E Hasselmo. 2007. “Temporal Frequency of Subthreshold Oscillations Scales with Entorhinal Grid Cell Field Spacing.” *Science (New York, N.Y.)* 315(April): 1719–22.

Hasselmo, Michael E, and Mark P Brandon. 2008. “Linking Cellular Mechanisms to Behavior: Entorhinal Persistent Spiking and Membrane Potential Oscillations May Underlie Path Integration, Grid Cell Firing, and Episodic Memory.” *Neural plasticity* 2008: 658323. http://www.pubmedcentral.nih.gov/articlerender.fcgi?artid=2480478&tool=pmcentrez&rendertype=abstract (July 16, 2014).

Higgs, M. H., and W. J. Spain. 2009. "Conditional Bursting Enhances Resonant Firing in Neocortical Layer 2-3 Pyramidal Neurons." *Journal of Neuroscience* 29(5): 1285–99. http://www.jneurosci.org/cgi/doi/10.1523/JNEUROSCI.3728-08.2009.

Hutcheon, B, and Y Yarom. 2000. "Resonance, Oscillation and the Intrinsic Frequency Preferences of Neurons." *Trends in neurosciences* 23(5): 216–22. http://www.ncbi.nlm.nih.gov/pubmed/10782127 (February 27, 2018).

Jeewajee, A., C. Barry, J. O'Keefe, and N. Burgess. 2008. "Grid Cells and Theta as Oscillatory Interference: Electrophysiological Data from Freely Moving Rats." *Hippocampus* 18(12): 1175–85.

Justus, Daniel et al. 2016. "Glutamatergic Synaptic Integration of Locomotion Speed via Septoentorhinal Projections." *Nature Neuroscience* 20(1): 16–19. http://www.nature.com/doifinder/10.1038/nn.4447.

Kropff, Emilio, James E. Carmichael, May-Britt Moser, and Edvard I. Moser. 2015. "Speed Cells in the Medial Entorhinal Cortex." *Nature* 523(7561): 419–24. http://www.nature.com/doifinder/10.1038/nature14622.

McNaughton, Bruce L. et al. 2006. "Path Integration and the Neural Basis of the 'Cognitive Map.'" *Nature Reviews Neuroscience* 7(8): 663–78. http://www.nature.com/doifinder/10.1038/nrn1932.

Migliore, M. et al. 1995. "Computer Simulations of Morphologically Reconstructed CA3 Hippocampal Neurons." *Journal of Neurophysiology* 73(3): 1157–68. http://www.ncbi.nlm.nih.gov/pubmed/7608762 (July 8, 2018).

———. 2006. "Parallel Network Simulations with NEURON." *Journal of Computational Neuroscience* 21(2): 119–29. http://link.springer.com/10.1007/s10827-006-7949-5 (July 8, 2018).

Mishra, Poonam, and Rishikesh Narayanan. 2014. "High-Conductance States and A-Type K+ Channels Are Potential Regulators of the Conductance-Current Balance Triggered by HCN Channels." *Journal of neurophysiology* 113(1): 23–43. http://www.ncbi.nlm.nih.gov/pubmed/25231614.

Moser, Edvard I, Emilio Kropff, and May-Britt Moser. 2008. "Place Cells, Grid Cells, and the Brain's Spatial Representation System." *Annual review of neuroscience* 31: 69–89.

Narayanan, Rishikesh, and Daniel Johnston. 2008. "The Ascent of Channels with Memory." *Neuron* 60(5): 735–38. http://www.ncbi.nlm.nih.gov/pubmed/19081367 (November 23, 2014).

Navratilova, Zaneta et al. 2012. "Phase Precession and Variable Spatial Scaling in a Periodic Attractor Map Model of Medial Entorhinal Grid Cells with Realistic after-Spike Dynamics." *Hippocampus* 22(4): 772–89.

Nolan, M. F., J. T. Dudman, P. D. Dodson, and B. Santoro. 2007. "HCN1 Channels Control Resting and Active Integrative Properties of Stellate Cells from Layer II of the Entorhinal Cortex." *Journal of Neuroscience* 27(46): 12440–51. http://www.jneurosci.org/cgi/doi/10.1523/JNEUROSCI.2358-07.2007.

Pastoll, Hugh, Melanie White, and Matthew Nolan. 2012. "Preparation of Parasagittal Slices for the Investigation of Dorsal-Ventral Organization of the Rodent Medial Entorhinal Cortex." *Journal of visualized experiments : JoVE* e3802(61): 1–9. http://www.ncbi.nlm.nih.gov/pubmed/22491152.

Quilichini, Pascale, Anton Sirota, and György Buzsáki. 2010. "Intrinsic Circuit Organization and Theta-Gamma Oscillation Dynamics in the Entorhinal Cortex of the Rat." *The Journal of neuroscience : the official journal of the Society for Neuroscience* 30(33): 11128–42. http://www.pubmedcentral.nih.gov/articlerender.fcgi?artid=2937273&tool=pmcentrez&rendertype=abstract (November 19, 2014).

Reifenstein, E. T. et al. 2016. "Cell-Type Specific Phase Precession in Layer II of the Medial Entorhinal Cortex." *Journal of Neuroscience* 36(7): 2283–88. http://www.jneurosci.org/cgi/doi/10.1523/JNEUROSCI.2986-15.2016.

Remme, Michiel W H, Máté Lengyel, and Boris S. Gutkin. 2010. “Democracy-Independence Trade-off in Oscillating Dendrites and Its Implications for Grid Cells.” *Neuron* 66(3): 429–37.

Richardson, Magnus J E, Nicolas Brunel, and Vincent Hakim. 2003. “From Subthreshold to Firing-Rate Resonance.” *Journal of neurophysiology* 89(5): 2538–54. http://www.ncbi.nlm.nih.gov/pubmed/12786187.

Schmidt-Hieber, C., and M. Hausser. 2013. “How to Build a Grid Cell.” *Philosophical Transactions of the Royal Society B: Biological Sciences* 369(1635): 20120520–20120520. http://rstb.royalsocietypublishing.org/cgi/doi/10.1098/rstb.2012.0520.

Schmidt-Hieber, Christoph, and Michael Häusser. 2013. “Cellular Mechanisms of Spatial Navigation in the Medial Entorhinal Cortex.” *Nature Neuroscience* 16(3): 325–31. http://www.nature.com/doifinder/10.1038/nn.3340.

Sinha, Manisha, and Rishikesh Narayanan. 2015. “HCN Channels Enhance Spike Phase Coherence and Regulate the Phase of Spikes and LFPs in the Theta-Frequency Range.” *Proceedings of the National Academy of Sciences*: 201419017. http://www.pnas.org/lookup/doi/10.1073/pnas.1419017112.

Sreenivasan, Sameet, and Ila Fiete. 2011. “Grid Cells Generate an Analog Error-Correcting Code for Singularly Precise Neural Computation.” *Nature Neuroscience* 14(10): 1330–37. http://www.nature.com/articles/nn.2901 (February 27, 2018).

Stark, Eran et al. 2013. “Inhibition-Induced Theta Resonance in Cortical Circuits.” *Neuron* 80(5): 1263–76.

Sun, Chen et al. 2015. “Distinct Speed Dependence of Entorhinal Island and Ocean Cells, Including Respective Grid Cells.” *Proceedings of the National Academy of Sciences*: 201511668. http://www.pnas.org/content/early/2015/07/08/1511668112.abstract (July 15, 2015).

Tang, Qiusong et al. 2014. “Pyramidal and Stellate Cell Specificity of Grid and Border Representations in Layer 2 of Medial Entorhinal Cortex.” *Neuron* 84(6): 1191–97. http://dx.doi.org/10.1016/j.neuron.2014.11.009.

Tennant, Sarah A et al. 2018. “Stellate Cells in the Medial Entorhinal Cortex Are Required for Spatial Learning.” *Cell reports* 22(5): 1313–24. http://www.ncbi.nlm.nih.gov/pubmed/29386117 (July 1, 2018).

Uebachs, M. et al. 2010. “Efficacy Loss of the Anticonvulsant Carbamazepine in Mice Lacking Sodium Channel Subunits via Paradoxical Effects on Persistent Sodium Currents.” *Journal of Neuroscience* 30(25): 8489–8501. http://www.jneurosci.org/cgi/doi/10.1523/JNEUROSCI.1534-10.2010 (July 8, 2018).

Supplementary figures

1.

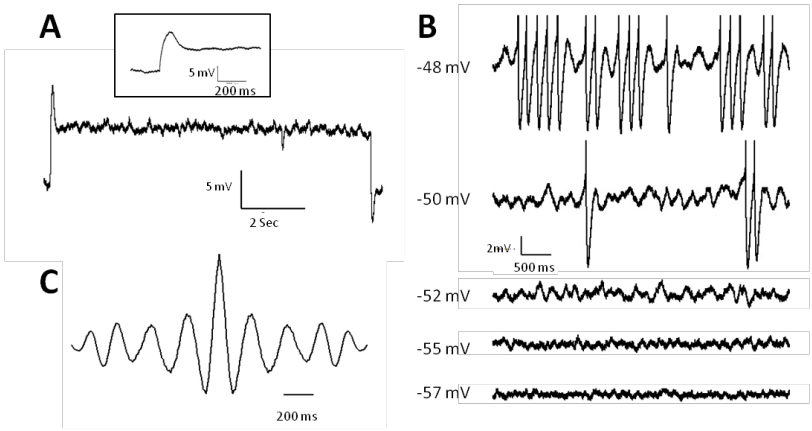

2.

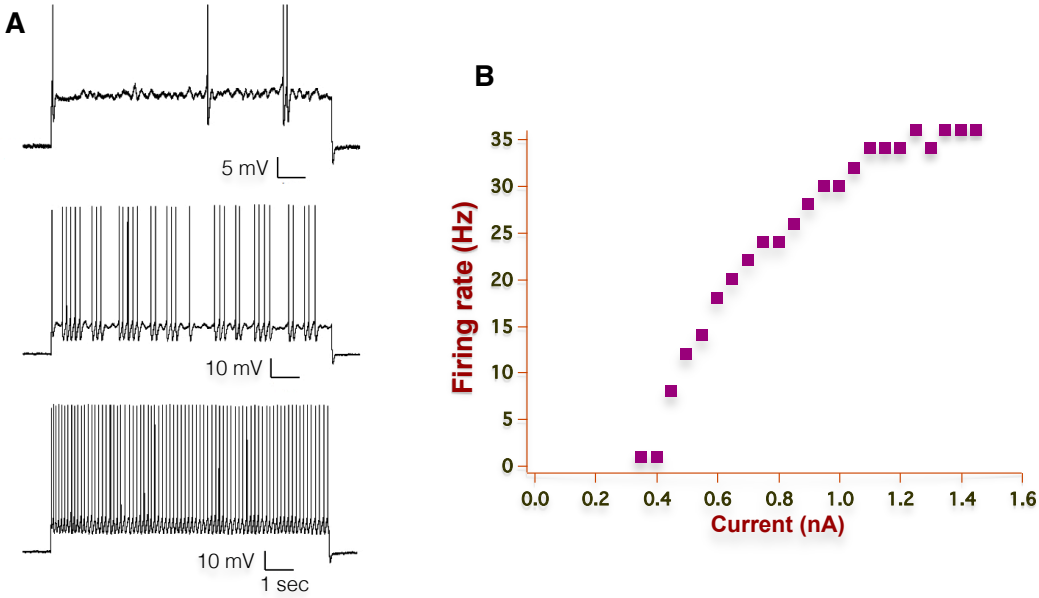

3.

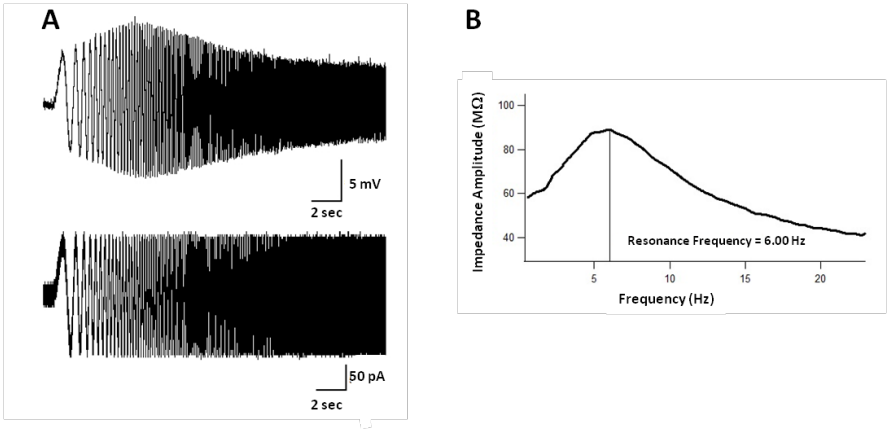

Fig S1. Electrophysiological characterization of the stellate cells

1. **Subthreshold Responses to depolarizing pulses.** A. Voltage response to a 12 sec. long pulse showing sag in the depolarizing direction (expanded in the inset) at the pulse onset, followed by oscillatory activity. B. Subthreshold oscillations start developing at around -57 mV and increase in amplitude with further depolarization. Intermittent spikes separated by few cycles of oscillations can be observed at more depolarized levels. C. Autocorrelation of a 1 sec segment at -50 mV form B, showing the rhythmic nature.
2. **Suprathreshold membrane potential responses.** A. Voltage responses to 10 sec long current pulses of 0.16nA (top), 0.19nA (middle) and 0.22 nA (bottom) in amplitude. Subthreshold oscillations can be seen to predominate at lower levels of injected current, followed by clustered spiking at subsequent higher current injections. Regular spiking is observed with further increase in amplitude of the injected current (0.22 nA in this case, approx. 0.4 – 0.6 nA for most of the cells). B. Frequency Vs. Injected current (F-I) plot. The type II nature is evident from absence of firing in the lower frequencies. (The data points at 1 Hz are the initial bursts).
3. **Response to chirp stimulus.** A. Selective amplification of voltage in response to a chirp stimulus spanning 25 Hz in 25 sec. Initial 15 ms trace is shown. B. Resonance frequency is the chirp stimulus frequency for which the Impedance amplitude is the maximum (6 Hz in this case).

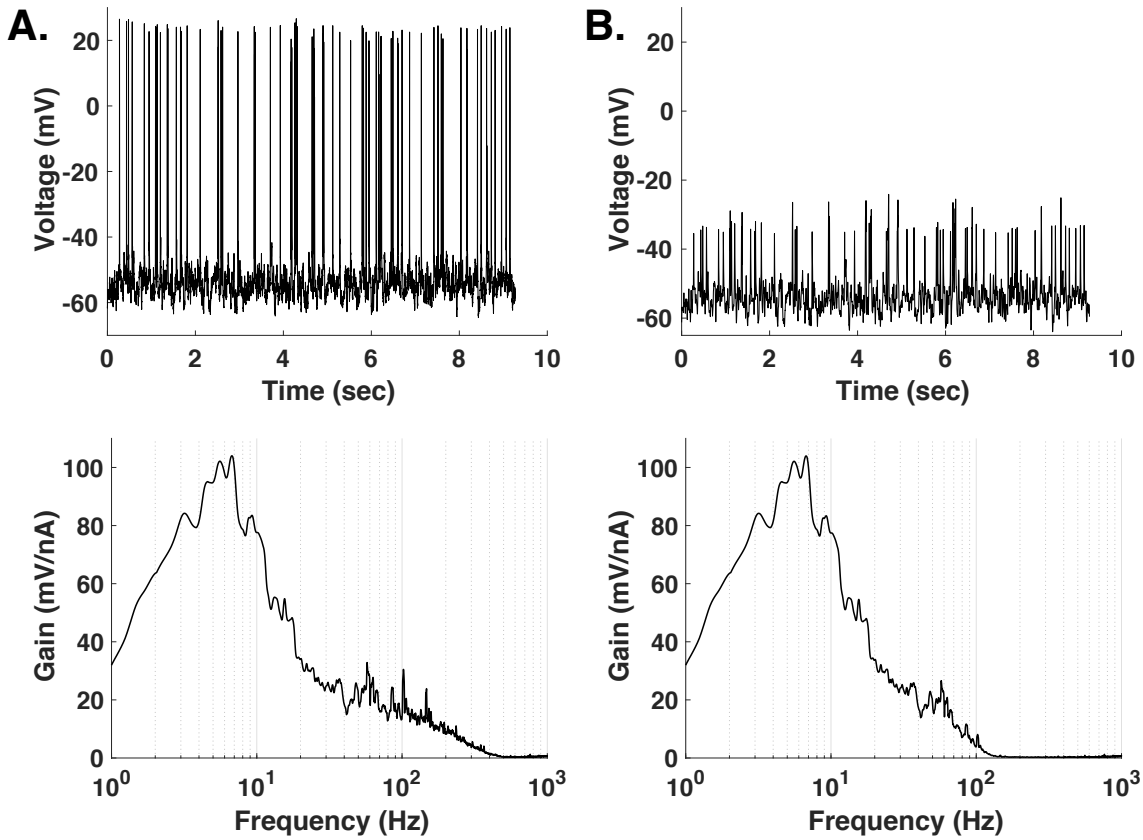

Fig. S2 Contribution of spikes to the $Gain_V$ waveform

A. $Gain_V$ waveform (bottom) with the original collective voltage trace (Top) for a single trial.
B. Same as A, after attenuation of spikes.

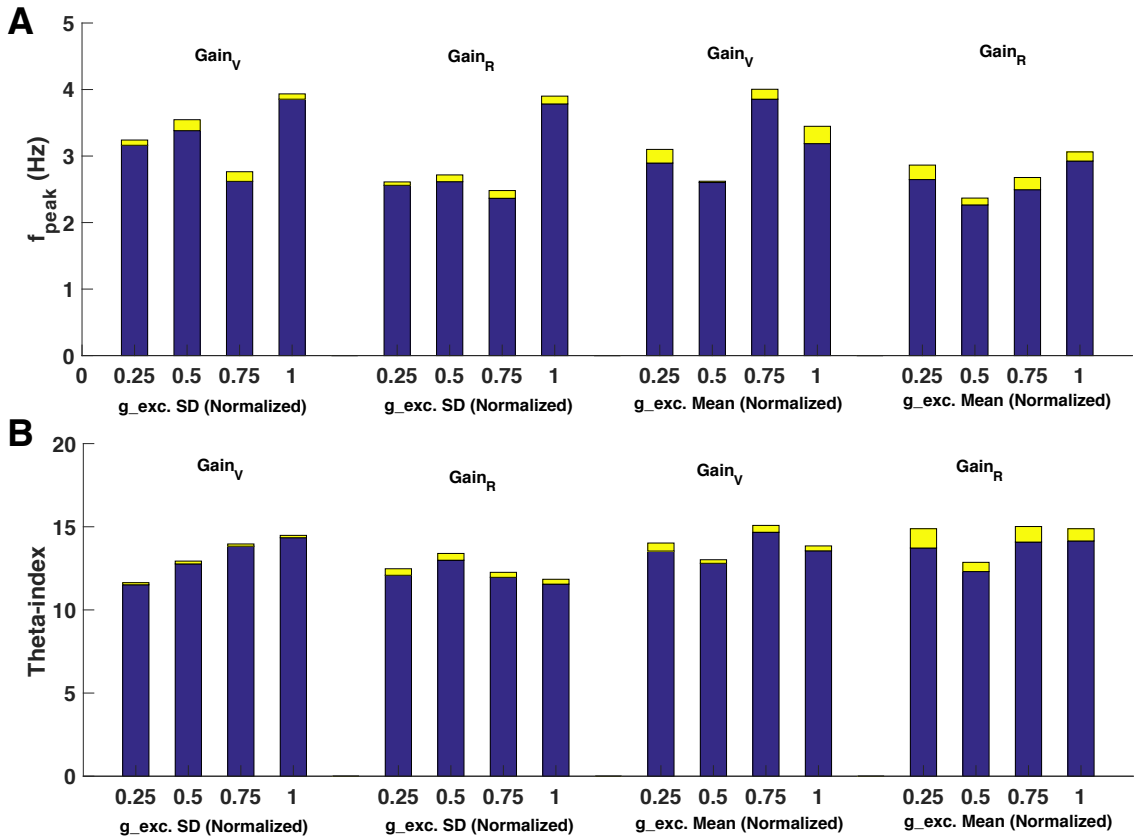

Fig. S3 Effects of stimulus statistics on the signal gain in the presence of ZD.
A. Gain$_V$ and Gain$_R$ peak frequency as a function of increase in the SD or Mean of the excitatory conductance, in the presence of ZD7288.
B. Gain$_V$ and Gain$_R$ theta-index as a function of increase in the SD or Mean of the excitatory conductance, in the presence of ZD7288.

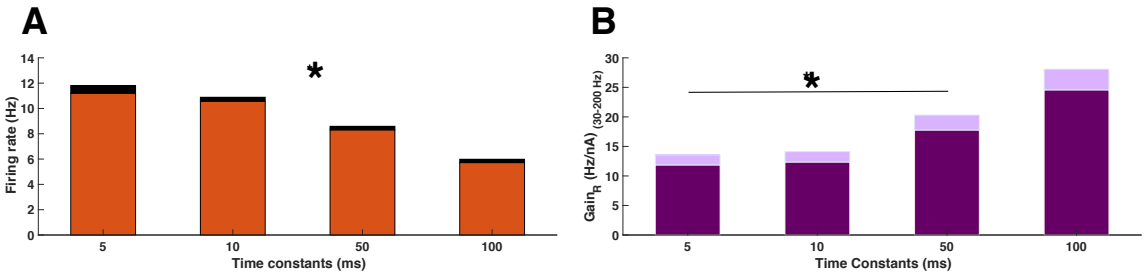

Fig. S4 Effect of stimulus kinetics on the firing rate and gamma frequency Gain$_R$
A. Firing rate as a function of time constants of the exitatory and inhibitory conductances.
B. Average Gain$_R$ in gamma frequency (30-200 Hz) as a function of time constants of the exitatory and inhibitory conductances.
A,B: * $p < 0.05$, Kruscal-Wallis test

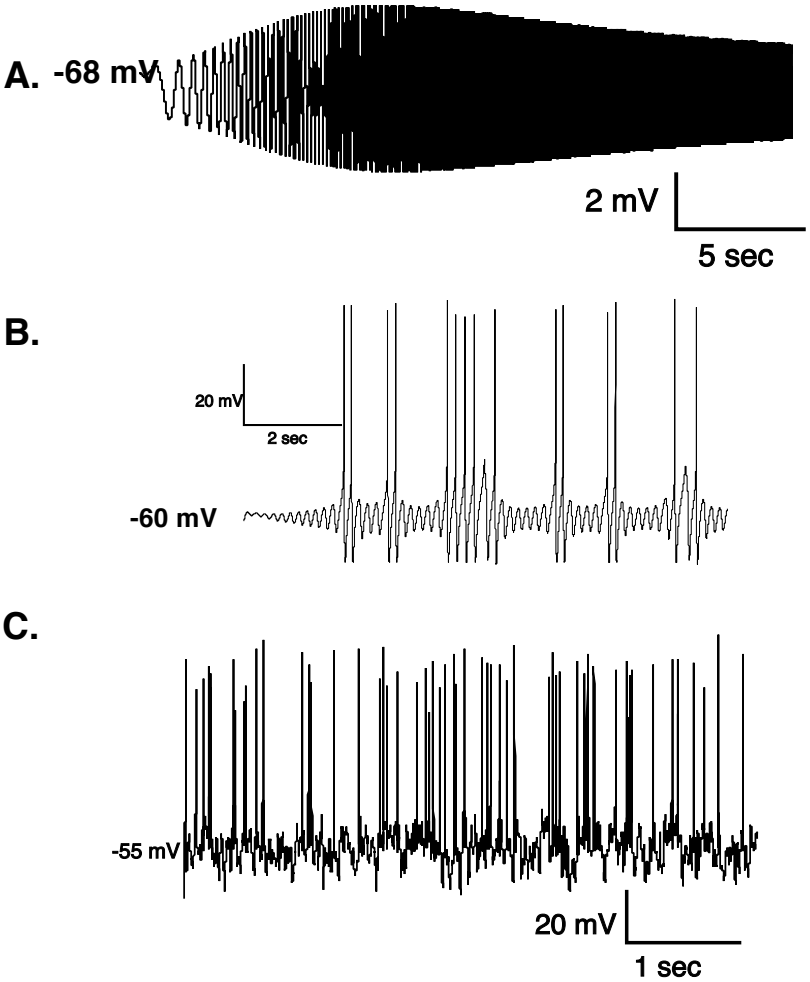

Fig. S5 Verification of the stellate cell electrophysiological features in the computational model

A. Voltage response of the model Stellate cell to a 0.1 nA chirp stimulus spanning 25 Hz in 25 sec, exhibiting theta-frequency resonance.

B. Subthreshold oscillations and spike clustering in response to a 1.7 nA stimulus from The baseline at -75 mV

C. Spontaneous theta frequency firing in the model stellate cell, in the in-vivo regime.

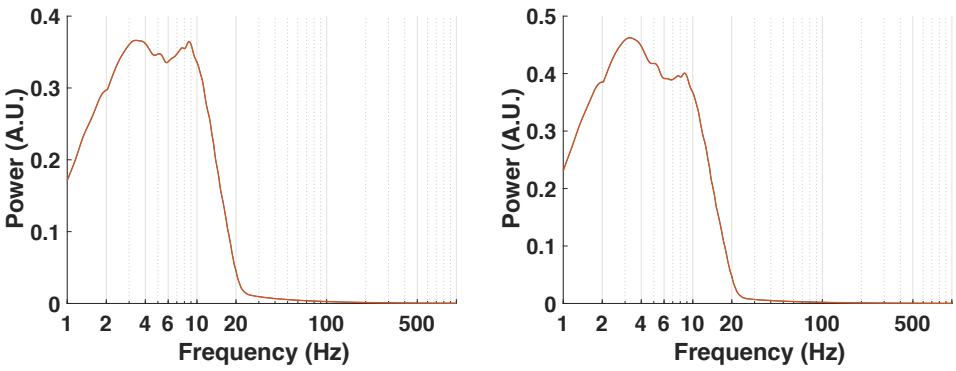

Fig. S6 Theta modulation of inputs by HCN channels in the model stellate cell

Left: Power spectrum of the 4-15 Hz filtered theta signal in the presence (Left), and absence of HCN (Right).